nature reviews bioengineering

https://doi.org/10.1038/s44222-022-00014-4

Review article

Check for updates

Bioinspired chiral inorganic nanomaterials

Nam Heon Cho[1], Andrés Guerrero-Martínez[2], Jessica Ma[3,4,5], Sara Bals[6,7], Nicholas A. Kotov[3,4,5] ✉, Luis M. Liz-Marzán[8,9,10] ✉ & Ki Tae Nam[1] ✉

Abstract

From small molecules to entire organisms, evolution has refined biological structures at the nanoscale, microscale and macroscale to be chiral—that is, mirror dissymmetric. Chirality results in biological, chemical and physical properties that can be influenced by circularly polarized electromagnetic fields. Chiral nanoscale materials can be designed that mimic, refine and advance biological chiral geometries, to engineer optical, physical and chemical properties for applications in photonics, sensing, catalysis and biomedicine. In this Review, we discuss the mechanisms underlying chirality transfer in nature and provide design principles for chiral nanomaterials. We highlight how chiral features emerge in inorganic materials during the chemical synthesis of chiral nanostructures, and outline key applications for inorganic chiral nanomaterials, including promising designs for biomedical applications, such as biosensing and immunomodulation. We conclude with an outlook to future opportunities and challenges, including the need for refined characterization techniques.

Sections

[1]Department of Materials Science and Engineering, Seoul National University, Seoul, South Korea. [2]Departamento de Química Física, Universidad Complutense de Madrid, Madrid, Spain. [3]Department of Chemical Engineering, University of Michigan, Ann Arbor, MI, USA. [4]Department of Materials Science, University of Michigan, Ann Arbor, MI, USA. [5]Biointerfaces Institute, University of Michigan, Ann Arbor, MI, USA. [6]Electron Microscopy for Materials Science (EMAT), University of Antwerp, Antwerp, Belgium. [7]NANOlab Center of Excellence, University of Antwerp, Antwerp, Belgium. [8]CIC biomaGUNE, Basque Research and Technology Alliance (BRTA), Donostia-San Sebastián, Spain. [9]Ikerbasque, Basque Foundation for Science, Bilbao, Spain. [10]CINBIO, University of Vigo, Vigo, Spain.
✉e-mail: kotov@umich.edu; llizmarzan@cicbiomagune.es; nkitae@snu.ac.kr

Introduction

Bioengineering has long been inspired by nature, primarily at the macroscale[1–4]. The development of powerful structure elucidation techniques[5,6] has further enabled the engineering and design of materials at the nanoscale, aiming at atomic precision[7–9]. Given the abundance of nanostructures in biology[10,11], nanoengineering naturally enters the realm of biomimicry of natural nanoscale systems[10,12–14]. As exemplified by nacre-like nanocomposites, bioinspired nanostructures have become a driver for progress in multiple materials and devices, enabling various energy technologies[15–17] and inspiring the rapid development of skin-like electronics. The key strategies in the design of bioinspired materials are broad utilization of the universal ability of nanoparticles to self-organize[18,19] and versatile combination of nanoscale biological species, inorganic nanoparticles and abiological macromolecules[20–22]. For these reasons, device fabrication and technological translation have been drastically accelerated owing to simplified processability[23–25], which involved the spontaneous emergence of multiple scales of organization, starting from molecular interactions[26,27] and developing into complex nanoscale, microscale and macroscale patterns with various levels of complexity[28,29]. Bioinspired nanomaterials could thus mimic, refine and advance the variety of materials engineered by nature[30–32].

The majority of biomolecules and their assemblies (for example, proteins and DNA) have a basic and common geometrical feature: chirality, also known as mirror dissymmetry[33]. Chirality is defined as the geometrical property of an object whose mirror image cannot be brought to coincide with itself[34–38] (Box 1). Chiral objects or ensembles of objects must also not contain any improper rotation axes, such as reflection planes and inversion centres[36]. Unlike macroscopic systems (for example, hands), direct evaluation of the mirror asymmetry of shapes in biomolecules is not straightforward owing to their dynamic and complex structure[38], as well as the limited spatial resolution of imaging systems. Albeit imperfect, circular dichroism spectroscopy—that is, the difference in the extinction of left and right circularly polarized light (CPL)[39]—is often used to assess the chirality of chemical and biological systems, for example to evaluate the secondary structure, folding and binding of proteins[40].

Chirality, which is present across all size scales in nature, leads to biological, chemical and physical properties that may be influenced by circularly polarized electromagnetic fields[41,42]. For example, chiral light and surface catalytic activity have been proposed as the symmetry-related underlying causes of homochirality in the origin of life[43]. Therefore, chirality can be considered as a foundational bioinspired principle for engineering[44,45], for example to design biosensors[46], or to realize a negative refraction index[47] at selected regions of the electromagnetic spectrum in chiral inorganic nanomaterials[48], which demands intense optical activity in conjunction with a high degree of transparency[49].

Bioinspired chiral nanomaterials are ideal for bio-physico-chemical applications, such as sensing and catalysis, in which selectivity and specificity arise as differentiating elements in comparison with non-chiral nanomaterials[50–53]; however, the mechanisms underlying chirality transfer processes in the preparation of inorganic nanomaterials with inherent chirality, from molecular to macroscale levels, are not sufficiently understood. Therefore, it is crucial to extract and unify lessons from biological examples of chirality transfer and determine how these criteria may guide the design of chiral inorganic nanomaterials.

In this Review, we highlight the mechanisms underlying the generation of chirality in biology, and discuss synthetic principles of bioinspired chiral inorganic nanomaterials, excluding (bio) organic–inorganic hybrid systems (for example, self-assembled nanostructures). We describe hierarchical multiscale chirality in biological systems (for example, cytoskeleton hypothesis and chirality in biominerals), and analyse the most abundant chirality transfer mechanisms in biology, including enantioselective interaction between surfaces and chiral molecules, template-induced synthesis and chirality transfer, and photon-induced chiral nanomaterials. However, as in many natural systems[54], these transfer mechanisms cannot be analysed separately because a concomitance of effects is responsible for the resulting chiral morphologies, in particular for highly crystalline nanomaterials, for which template-induced and photon-induced syntheses cannot be entirely decoupled from enantioselective interactions at high Miller index surfaces. Finally, we present potential applications in photonics (for example, polarization-control, non-linear optics), sensing (enantiomer discrimination), catalysis (chemical and pharmaceutical) and biomedicine (for example, photothermal and photodynamic therapies).

Chirality in biology

Chirality exists across multiple size scales in biological entities, dictating their geometries, properties and behaviour. For example, aminoacyl-tRNA synthases, enzymes involved in the selection of amino acids in protein synthesis, preferentially bind to L-amino acids by steric exclusion of D-amino acids[55]. Peptide elongation of D-amino acids at the ribosomes is slow owing to the large distance between the reaction sites[56], limiting the production of peptides with incorporated D-amino acids[57,58]. The incorporation of some D-amino acids, such as D-Asp and D-Ser, has been linked to amyloid-β peptides present in the brains of patients with Alzheimer disease[59], indicating that chirality at the molecular level could extend its influence to the organism and its behaviour.

Chirality also offers survival advantage(s) for organisms. Fan-like petal arrangements of mutated *Arabidopsis thaliana* show left-handed chirality and clockwise twisting. The handedness of their asymmetric geometry is fixed in certain species, indicating that their chirality is genetically encoded[60–62] (Fig. 1a,b). Although these plants normally grow straight, mutations affecting the microtubules, such as SPIRAL1, SPIRAL2 or SPIRAL3, as well as microtubule-depolymerizing drugs, such as propyzamide, cause helical growth owing to an asymmetric elongation of cells[60]. Spiral growth in the elongating organs is induced by the dominant-negative mutations at the tubulin intra-dimer interface. Mutation at α-tubulins 4 and 6 further decreases microtubule stability, inducing left-handed organ twisting in *Arabidopsis*[61]. Moreover, structural chirality substantially affects the mechanistic behaviour of organisms. For example, in *Drosophilia*, the chiral interaction of the molecular motors myosin 1D and f-actin mediates the directional twisting of cells, organs and the entire organism[63]. In *Escherichia coli*, the asymmetry in flagella movements allows the bacteria to both change direction and propel themselves forward[64,65]. Individuals swim by rotating their flagella anticlockwise[64,66], and counteract the generated torque by rotating their cell body in the opposite direction. A combination of wall effects, flow effects and flow–wall coupling also allows bacteria to orient themselves and swim in a stable fashion[67]. Near a surface, these effects cause flagella to rotate clockwise[68], leading to a tumbling motion of *E. coli*[64,65].

The light polarization effects of chiral structures can also provide proliferation advantages. For example, the beetle *Chrysina gloriosa* shows different iridescence colours under unpolarized light and with either left or right-polarized light (Fig. 1c). The exoskeleton of *C. gloriosa* possesses hexagonally patterned cellular structures, with

Box 1

Chirality

Chirality refers to a geometrical property when an object cannot be superimposed onto its mirror image[35]. Similarly, an object is achiral if its mirror image can be brought to coincide with itself. Chirality is common in both biological and abiological matter. For example, the amino acid glycine is achiral, whereas its homologue alanine is chiral because it has an asymmetric carbon (a carbon atom that is attached to four different types of atoms or groups of atoms) (see the figure, panel **a**). A chiral molecule and its mirror image constitute an isomer pair, that is, enantiomers. Enantiomers can rotate the polarization of light into a certain inverse direction with the same intensity[37].

Chirality can also be described in the framework of group theory; here, an object (for example, a molecule) can be chiral if, and only if, it does not contain improper rotation axes (S_n) in its structure[36]. This symmetry operation involves two consecutive transformations: the first is a rotation of $360/n°$, and the second is a reflection through a plane perpendicular to the previous rotation axis. For example, systems with a regular tetrahedral symmetry present three improper rotation axes S_4 (see the figure, panel **b**), which can be decomposed in a 90° rotation (C_4) followed by a reflexion through a horizontal plane (σ_h) (see the figure, panel **c**). Therefore, a tetrahedron molecule with A=B=C=D, such as CH_4, is not chiral, whereas a molecule with an asymmetric carbon, where A≠B≠C≠D, is chiral (see the figure, panel **a**). Thus, all objects with planes of reflection (S_1=σ) and/or centres of inversion (S_2=i) are achiral. By contrast, objects with point groups C_1, C_n and D_n can be chiral. These spatial criteria allow the construction of multifunctional biological nanostructures, and can also be applied for the design of bioinspired chiral inorganic nanomaterials, for example dissymmetric tetrapods, anisotropic junctions or helical conformations (see the figure, panel **d**), as well as other (bio)organic–inorganic hybrid systems (for example, self-assembled nanostructures, such as tetrahedral assemblies or helical arrangements of nanoparticles) (see the figure, panel **e**). Parts **d** and **e** reprinted with permission from ref. 38, Elsevier.

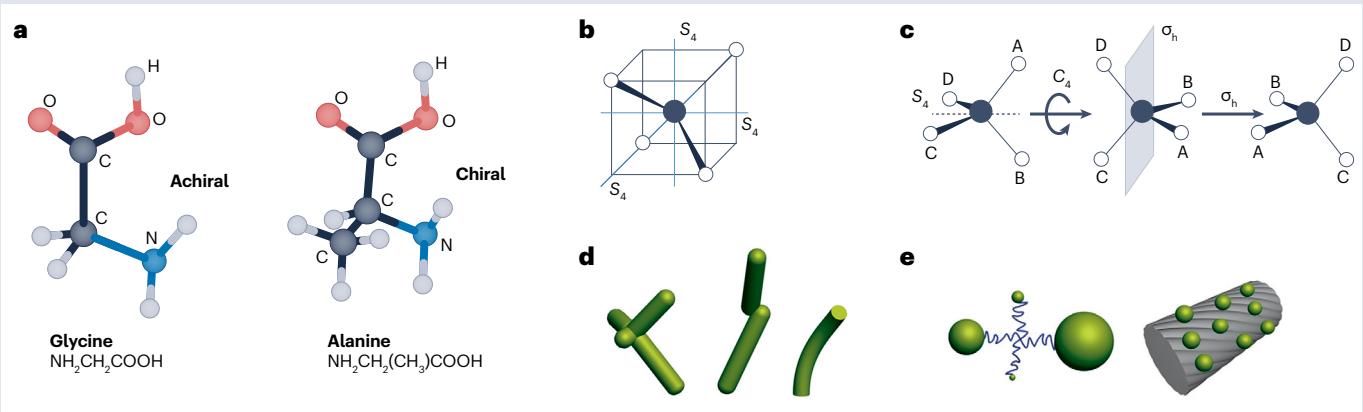

each cell containing a chiral nematic liquid crystal-like conical peak surrounded by nested arcs. Although each layer is organized along a single direction, the stacked layers form a helical Bouligand structure[42]. With such an exoskeleton, *C. gloriosa* selectively reflects left CPL to exhibit a bright metallic green colour that dims upon irradiation of light with right circular polarization[42,69]. Interestingly, *C. gloriosa* can visually differentiate reflected polarized light as a method of communication[70]. Similar Bouligand structures are found in many other chitinous exoskeletons[71,72], for example in the mantis shrimp shell[73]. The circular polarization vision of stomatopod crustaceans or the mantis shrimp illustrates how organisms differentiate and use polarization-dependent optical properties. The eyes of stomatopods have high degrees of rotational freedom. By torsional rotation of their eyes, orthogonally arranged stacked layers of retinular cells in the rhabdom differentiate the polarization state of light. Furthermore, differentiating the iridescence of the telson keel under polarized light is a sex-specific behaviour; here, reflection of CPL is only observable in males (Fig. 1d). The ability to detect and analyse CPL is suggested to mediate mate signalling and to enhance contrast in turbid environments[74,75]. Bones[76], the dermal armour of *Arapaima gigas*[77], and *Pollia condensata* fruits[78] also contain chiral nanostructures to improve mechanical properties.

To mimic and exploit chiral nanostructures of plants, animals and inorganic tissues for the design of nanomaterials, their evolutionary mechanism needs to be understood. The formation of asymmetry at the macroscale is often a result of chirality transfer from small to large scales, for which the nanoscale plays a crucial role[79]. In nature, the generation of chirality is based on hierarchy, with chiral superstructures displaying chirality at the molecular, nanoscale, microscale and macroscale. For example, the tendrils of climbing plants show helical growth by attaching their aerial axial organs to the nearby support for vertical growth and enhanced exposure to sunlight[80,81]. Similarly, chirality in towel gourds is hierarchical, spanning over at least six length scales from the molecular to the macroscopic level. At the molecular level, cellulose is made of chiral sugar molecules. The cellulose forms stiff and helical microfibrils, which enable swelling and deswelling of tendrils in water, resulting in a change of the fibril helical angle, which causes

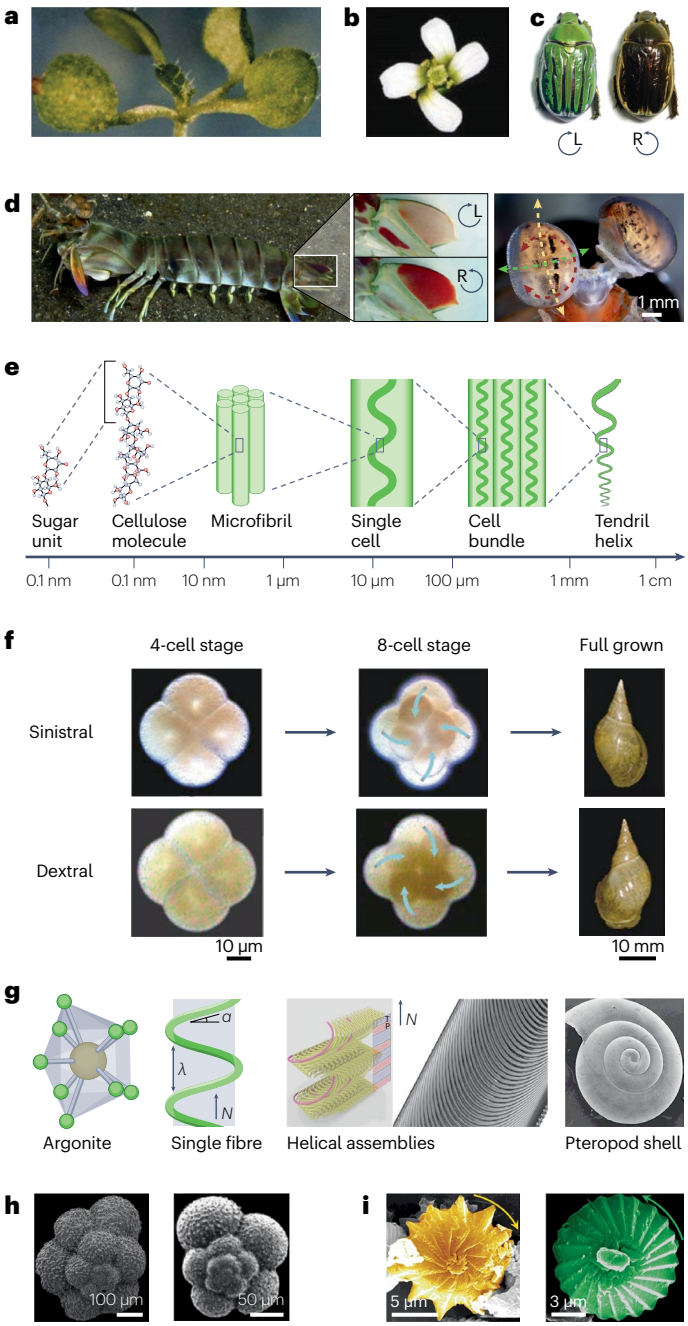

Fig. 1 | Chirality in biology. a, The cotyledons and first leaves of the SPIRAL2 mutant of *Arabidopsis thaliana* show counter-clockwise rotation[60]. **b**, Flowers of the SPIRAL2 mutant of *A. thaliana* also show counter-clockwise rotation[60]. **c**, The exoskeleton of *Chrysina gloriosa* is green under left-handed circularly polarized light (CPL), but gold under right-handed CPL[42]. **d**, The tail of the male *Odontodactylus cultrifer* shrimp appears differently saturated under left and right CPL. The eye of these mantis shrimps are able to adjust pitch, yaw and torsional rotation. Torsional rotation allows the shrimp to align its eyes with the polarization of incident light[74,75]. **e**, Hierarchical chirality in a plant tendril. Sugar is the building block of cellulose, which is formed into chiral microfibrils that transfer their chirality to the entire cell, cell bundles and the helical tendrils of *Luffa acutangular*[82]. **f**, The formation of dextral (right-handed) or sinistral (left-handed) forms in *Lymnaea stagnalis* is determined by the conformation of the cells in the snail embryo[83]. **g**, Chirality is transferred upwards from aragonite crystals to helical fibres, which stack parallel or transverse to each other to form a pteropod shell[88–90]. **h**, Chiral diversity of foraminifera skeletons. Clockwise rotation is found in animals living in high-temperate regions or tropical oceans, and counter-clockwise rotation is found in animals living in the Arctic and Antarctic oceans[91,92]. **i**, Coccolithophore skeletons show clockwise and counter-clockwise rotation[88]. Parts **a** and **b** adapted from ref. 60, CC BY 4.0 (https://creativecommons.org/licenses/by/4.0/). Part **c** is from Sharma, V., Crne, M., Park, J. O. & Srinivasarao, M. Structural origin of circularly polarized iridescence in jeweled beetles. *Science* **325**, 449–451 (2009). Reprinted with permission from AAAS. Part **d**, image courtesy of Christine Huffard. Part **d** adapted with permission from ref. 74, Elsevier. Part **d** adapted from ref. 75, Springer Nature Limited. Part **e** adapted from ref. 82, Springer Nature Limited. Part **f** adapted with permission from ref. 83, Elsevier. Part **g** adapted with permission from ref. 235, Elsevier. Part **g** adapted from ref. 86, Springer Nature Limited. Part **g** reprinted from ref. 90, Springer Nature Limited. Part **g** adapted with permission from ref. 89, Wiley. Part **h** adapted with permission from ref. 91, Elsevier. Part **h** reprinted with permission from ref. 92, the Geological Society. Part **i** adapted with permission from ref. 236, Ocean Drilling Program.

a torque on the cross section of the cells, forcing them to also take on a helical shape. Microscale bundles of chiral cells then group together to form the macroscopic helices of the towel gourd[82] (Fig. 1e). Hierarchical chirality transfer is also present in animals, for example, in *Lymnaea stagnalis* snails. Sinistral or dextral chirality in these organisms can already be observed at the four-cell stage, and during the third cleavage step, from the four-cell to the eight-cell stage, micromeres rotate anticlockwise and clockwise with respect to their sister macromeres. Such embryonic chirality determines the final sinistral or dextral adult snail shells, affecting their mating behaviour[83,84] (Fig. 1f). Similarly, the exoskeletons of ocean pteropods, such as *Limacina helicina*, have thin transparent shells that consist of microstructures made of aragonite crystal nanofibres with a right-handed orientation[85–88]. These helical nanofibres are densely packed to form a material that is tougher and more resistant to brittle failure than a shell made of straight fibres owing to the spring response of the coils[88–90] (Fig. 1g).

Chirality can also be transferred from organic molecules to macroscopic morphologies in inorganic materials. Although the underlying mechanisms remain to be confirmed, chirality can be transferred through molecular interactions at organic and inorganic interfaces and biological templates. For example, the calcium carbonate shell of the foraminifera *Globigerina pachyderma*, a single-cell marine microorganism, shows temperature-dependent handedness. The shell spirals clockwise in high-temperature and tropical regions, whereas it spirals counter-clockwise in the oceans near the Artic and the Antarctic[91,92] (Fig. 1h). Here, chiral aspartic acid (Asp) molecules generate the chiral morphologies, with enantioselective interactions of L-Asp inducing counter-clockwise rotation and D-Asp inducing clockwise rotation[93]. Asp interacts with the surface of calcite and alters the local free energy, resulting in the propagation of crystal growth in one direction or another[94]. *Herdmania momus* shows a similar molecular interaction-based control of macroscopic biomineral chirality. This ascidian contains an endoskeleton composed of vaterite[95], which is formed through addition of Asp or glutamic acid (Glu), causing a tilt of its hexagonal subunits. Addition of the D or L enantiomers of Asp and Glu leads to the hierarchical organization of the flat platelets, which grow in a right or left spiral pattern, respectively[96]. Coccolithophores, a group of

unicellular plant plankton, produce calcite-based exoskeletons, called coccoliths, which exist in both enantiomorph forms in nature[88] (Fig. 1i). The proposed chirality transfer mechanism involves a belt of chiral macromolecules surrounding the pre-existing exoskeleton during nucleation, dictating the binding sites for calcium or carbonate ions[97]. Furthermore, exoskeletons of the foraminifera *Orbulina universa* contain a primary organic sheet, composed of polysaccharides and acidic amino acids, which is produced during the initial stage of skeleton formation. Mineral growth occurs on both sides of this primary organic sheet, providing the template that guides the exoskeleton growth for *O. universa*[98].

Chirality transfer mechanisms

Mimicking biological chirality transfer mechanisms across multiple size scales and multiple materials groups may enable precise control of the geometric and physical properties of nanomaterials. For example, amplification of chirality transfer can be initiated from a small imbalance of symmetry in chiral catalysts to organic compounds[99]. In turn, a small imbalance in chirality can also induce substantial changes in the morphology of inorganic materials[100]. Nanoscale chirality can be induced in inorganic materials by assembly-based synthesis methods, such as DNA origami, or by self-assembly of achiral nanostructures[53,101,102]. Alternatively, artificial chiral inorganic nanomaterials with individual structural chirality can be synthesized using biological chirality transfer mechanisms, that is, enantioselective organic–inorganic interactions and chiral template-based chiral nanostructures. Exceeding the capability of nature, chiral nanomaterials have been designed that exploit a small enantiomeric imbalance in their response to photons to induce morphological chirality in inorganic nanomaterials (Table 1).

Enantioselective organic–inorganic interaction

Interactions at the organic–inorganic interface may show enantioselective behaviour, in which the molecular binding orientation, intensity or surface density might change with respect to the relative chirality of molecules and surfaces. In addition to molecular structures, inorganic crystal surfaces may feature chirality at the atomic level, with a lack of mirror symmetry perpendicular to the surface. For example, natural minerals, such as calcite, alkali feldspar and clinopyroxenes, possess enantiomorphic crystal facets[103,104]. Highly symmetric metal crystals are suggested to have chirality at high Miller index surfaces[105,106], that is, {*hkl*} ($h \neq k \neq l \neq 0$). Such surfaces possess atomically kinked sites composed of low-index crystal facets, such as {111}, {100} and {110}[107,108]. Atomic kink site chirality is defined by combining the rotational directionality of low-index crystal facets. In a few specific combinations of chiral crystal facets and chiral molecules, theoretical and experimental results show handedness-dependent changes in the surface orientation of chiral adsorbates on chiral crystal facets, leading to enantioselective surface interactions[103,105,109,110]. For example, on

Table 1 | Chiral inorganic nanostructures from different sources of chirality

Material	Source of chirality	Synthesis method	Ref.
Calcite crystals	Tartaric acid, malic acid, aspartic acid (Asp)	Electrochemical	115
Calcium carbonate	Asp, glutamic acid (Glu)	Chemical	96
Mercury sulfide	Penicillamine	Chemical	116
Cobalt oxide	Cysteine	Chemical	117
Cobalt oxide	Tyr-Tyr-Cys	Chemical	118
Tellurium, selenium	Glutathione, penicillamine	Chemical	120
Gold	Cysteine, glutathione	Chemical	133
Gold	Cysteine	Chemical	135
Gold	ssDNA+glutathione	Chemical	136
Gold	Cys-Gly	Chemical	137
Gold	ssDNA	Chemical	138
Palladium	Cysteine	Chemical	139
Silica	*N*-Miristoyl-L-alanine sodium salt	Chemical	151
Silica	CTAB+ammonia	Chemical	153
TiO_2	*N*-Stearoyl-L/D-glutamic acid	Chemical	155
Gold	CTAC+BINOL/BINAMINE	Chemical	160
CuO	*R*/*S*-2-Amino-3-phenyl-1-propanol	Hydrothermal	156
CdTe	CPL	Photochemical	169
Gold	Cysteine+CPL	Photochemical	170
Gold	Cysteine-based dipeptides+CPL	Photochemical	173
Gold+lead oxide	CPL	Photochemical	175
Gold	CPL	Photochemical	178

BINAMINE, 1,1′-binaphthyl-2,2′-diamine; BINOL, 1,1′-bi(2-naphthol); CdTe, cadmium telluride; CPL, circularly polarized light; CTAB, cetyltrimethylammonium bromide; CTAC, cetyltrimethylammonium chloride; ssDNA, single-stranded DNA.

Ag(643) and Cu(643) surfaces, a temperature-programmed desorption study revealed enantioselective adsorption behaviour of small chiral molecules, such as 2-butanol, propylene oxide and 3-methylcyclohexanone[109]. Furthermore, L-glucose shows higher electro-oxidation reactivity on Pt(643)^S surfaces than D-glucose. This enantioselective catalytic activity was related to the surface density of chiral atomic kink sites[106]. Enantioselective adsorption of chiral molecules could also reconfigure the atomic arrangement to imprint molecular chirality on inorganic surfaces. Through powder X-ray diffraction analysis of gold nanoparticles with adsorbed *p*-mercaptobenzoic acid, a chiral arrangement was determined for the atomic coordination at the unit-cell level[111]. The synthesis of cadmium telluride (CdTe) nanoparticles using L-cysteine-methyl-ester hydrochloride showed the preservation of a chiroptic response, even after replacement of chiral ligands with achiral ligands, indicating that adsorption of chiral molecules induces the irreversible development of atomic chirality[112]. Density functional theory simulations and corresponding Wulff thermodynamic structure reconstructions demonstrated the preferential binding of L-cysteine to Au(321) surfaces[113].

Enantioselective interactions between chiral molecules and inorganic surfaces have been proposed to induce macroscopic chirality in inorganic materials. During the synthesis of calcium carbonate, the introduction of chiral amino acids, such as Asp or Glu, induces a spiralling morphology. The resulting toroidal superstructure shows counter-clockwise spiral morphology upon addition of L enantiomers and clockwise spiral morphology upon addition of D enantiomers[96] (Fig. 2a). Calcium carbonate growth can be further extended using a single amino acid enantiomer, resulting in chirality switch, which is determined by the chiral interactions of constituent nanoparticles. The proposed chiral growth mechanism follows a sequential tilt of subunit structures upon addition of chiral molecules to the surface, starting from a platelet layer inclination stage and a platelet layer rotation stage. This finding provides a hypothesis to explain enantiomeric pairs in nature, despite the homochiral propensity of biological systems[114]. Introduction of chiral tartaric acid, malic acid and Asp during the electrochemical growth of calcite crystals also induces chiral morphologies. Here, the type of chiral molecule and its handedness control the final morphology of the calcite crystals[115] (Fig. 2a).

In addition to chiral biomineral suprastructures, inorganic chiral nanomaterials with macroscopic chiral morphologies can be synthesized in the presence of chiral biomolecules. For example, the twisted morphology of mercury sulfide (cinnabar) nanoparticles can be biased to the specific mirror asymmetric form using D- and L-penicillamine molecules attached to their surface. The primary chiral unit of the cinnabar α-HgS lattice, with a $P3_221$ space group, shows a helical arrangement of mercury and sulfur atoms along the crystallographic *c* axis. Here, the strong influence of molecular chirality on the crystallographic and geometric chirality of the nanoparticles was shown by two-step epitaxial growth[116] (Fig. 2b). Paramagnetic, chiral cobalt oxide (Co_3O_4) nanoparticle synthesis can also be based on chirality transfer from organic molecules to an inorganic crystal lattice, which causes chiral distortions. Interaction with chiral cysteine molecules generates chiral distortions in the crystal lattice of cobalt oxide, resulting in chiral phonons specific for the Co_3O_4 lattice[117]. Furthermore, the synthesis of cobalt nanoparticles using the chiral Tyr-Tyr-Cys peptide demonstrates the crucial role of the thiol group and carboxyl functional group for chirality evolution, on the basis of a 2D nuclear magnetic resonance study[118]. Similarly, colloidal II–VI semiconductor nanoplatelets with chiral helices can be synthesized with thiolated surface ligands[119]. The structure and composition of chiral molecules are key, as demonstrated in the synthesis of chiral tellurium and selenium nanoparticles. Chiral tellurium nanoparticles synthesized in the presence of chiral glutathione molecules show twisted ridges and triangular protrusions at each end of the nanoparticles. However, changes in the type of material and chiral molecules induce variations in the morphology and chiroptical response of the nanoparticles[120] (Fig. 2c). A more conservative role of chiral ligands has also been proposed. Thiolated penicillamine can be used in the synthesis of chiral tellurium nanoparticles with enantiomorphic chiral space groups of $P3_121$ and $P3_221$ (ref. 121). Interestingly, addition of achiral mercaptopropionic acid also yields similar chiral shapes of nanoparticles with equal enantiomeric ratio. Such chirality generation is attributed to screw dislocation at low-supersaturation growth conditions, with chiral ligands promoting handedness-biased synthesis. These various paths to chirality suggest that chirality transfer from small biomolecules provides a versatile route to constructing chiral inorganic materials.

Complex chiral morphologies can be obtained by controlling the adsorption of small chiral molecules on high Miller index surfaces. Various approaches have been proposed to precisely control exposed high Miller index facets in colloidal nanosynthesis[122,123], including chemical strategies. For example, seed-mediated growth, in which pre-synthesized nanoscale seeds are used to separate nucleation and growth stages, enables precise morphology control in a mild synthetic environment[124,125]. Here, the exposed facets in the nanoparticles and the resulting morphology are determined by the cooperative influence of thermodynamic and kinetic parameters. By balancing thermodynamic parameters, such as surface energies, adsorption energies of organic ligands and halide ions on the metal, and kinetic parameters, such as pH, reducing agents and temperature, the exposed facets can be precisely controlled[126–130]. Independent variation of reagent concentrations, such as the surfactant, seed nanoparticles, metal ion precursor and reducing agent, affects nanoparticle morphology. By controlling the reactants, rod, parallelepiped, hexagonal platelet, cube and multi-branched morphologies can be designed[131]. Thiol-containing organic molecules can also be used to control the morphology and exposed facets during gold nanoparticle synthesis. Using strong gold–sulfur bonding and the aromatic geometry of 4-aminothiophenol, concave rhombic dodecahedral nanoparticles can be synthesized that comprise various high-index facets, such as {331}, {221} and {533}. By tailoring the thiol surface ligands, other morphologies can be obtained, indicating the potential to further expand this synthetic methodology[132].

Uniform chiral gold nanoparticles with complex shapes can be grown using thiol-containing chiral amino acids or peptides in a seed-mediated synthesis[133]. Chiral surfaces of high-index facets preferentially interact with a chiral molecule of specific handedness. Preferential binding of molecules to the surface promotes an uneven elongation of the facet, which induces twisting of the nanoparticle geometry. Such evolution of twisted particle geometry follows the sequential trajectory of uniform high-index facet generation, tilting of edges for chiral motif formation and construction of well-defined boundaries with increased nanoparticle size[134]. Viewed from (110) and (100) directions, the introduction of cysteine molecules induces A′C and AC edge tilting in opposite directions, whereas the outer edges of A′C and AC shift towards the centre of the nanoparticle to create a chiral morphology. However, viewed from (110) and (100) directions, the introduction of cysteine-containing glutathione molecules induces contraction and protrusion of outer edges and pinwheel-like rotation of inner edges[133] (Fig. 2d). Owing to their 432 point group symmetry and

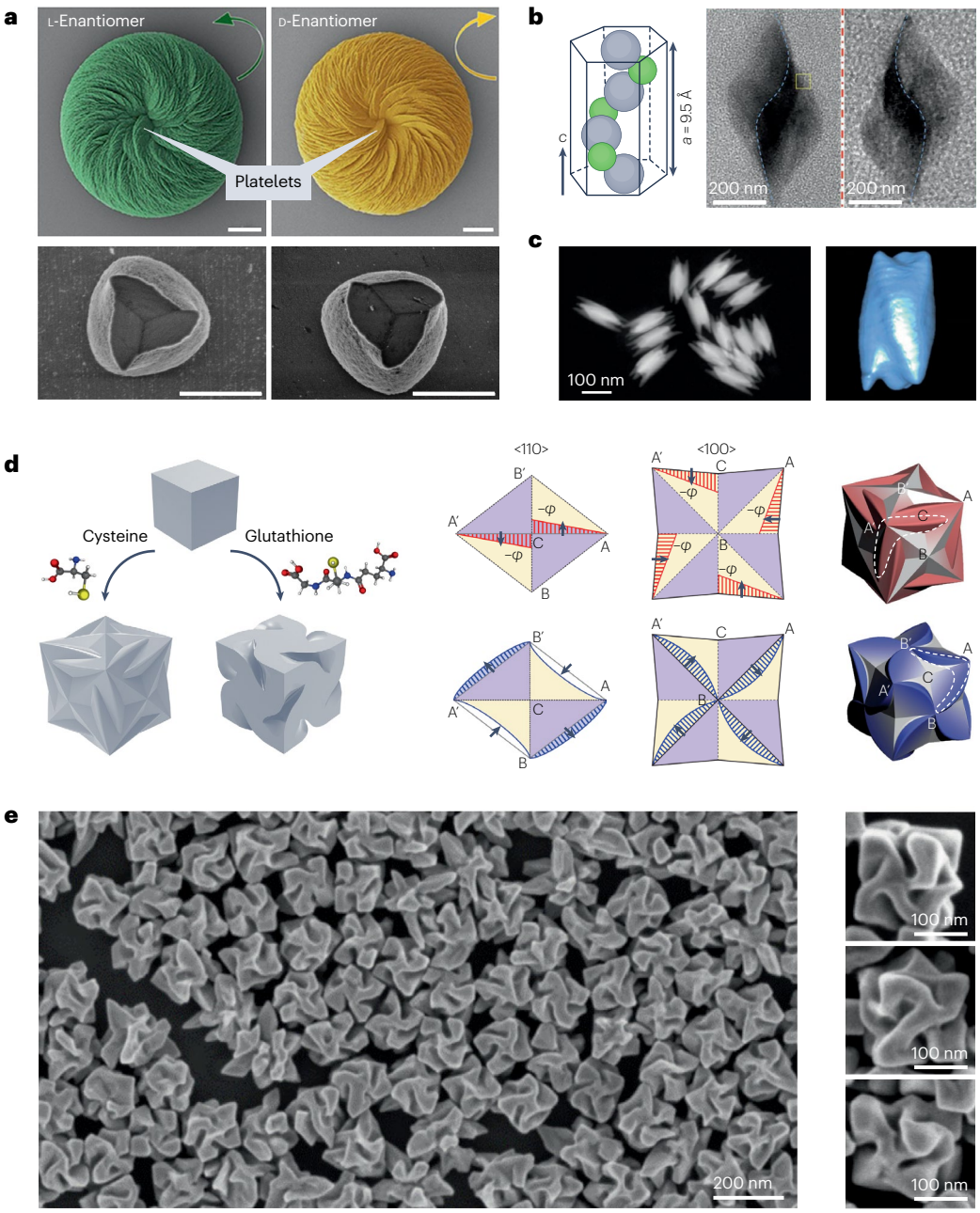

Fig. 2 | Chiral inorganic nanomaterials synthesized from enantioselective interaction. a, Scanning electron microscopy (SEM) images of chiral inorganic structures grown in L or D enantiomers[96]. Top: chiral vaterite microcrystals synthesized using L- or D-aspartic acid (Asp). Bottom: chiral calcite microcrystals synthesized using L- or D-tartaric acid[115]. Scale bar = 3 µm. **b**, Helical arrangement of atoms in a cinnabar HgS lattice along the crystallographic *c* axis and transmission electron microscopy (TEM) image of individual chiral nanostructures[116]. Scale bar = 200 nm. **c**, Scanning transmission electron microscopy (STEM) image and tomographic reconstruction of chiral tellurium nanoparticles. Scale bar = 100 nm. **d**, Morphology development of 432 helicoid nanoparticles with respect to types of input chiral molecules[133]. Introduction of cysteine molecules to cubic seed nanoparticles induces chiral nanoparticles with AC boundary tilting (depicted as red-coloured nanoparticles), whereas introduction of glutathione molecules to cubic seed nanoparticles leads to chiral nanoparticles with AB boundary tilting (depicted as a blue-coloured nanoparticles). **e**, Low-magnification and high-magnification SEM images of 432 helicoid III nanoparticles synthesized with octahedron seed nanoparticles and glutathione molecules[133]. High-magnification image scale bar = 100 nm. Part **a** adapted from ref. 96, Springer Nature Limited. Part **a** reprinted (adapted) with permission from Kulp, E. A. & Switzer, J. A. Electrochemical biomineralization: the deposition of calcite with chiral morphologies. *J. Am. Chem. Soc.* **129**, 15120–15121 (2007). Copyright 2007 American Chemical Society. Part **b** adapted from ref. 116, Springer Nature Limited. Part **c** reprinted from ref. 120, Springer Nature Limited. Parts **d** and **e** adapted from ref. 133, Springer Nature Limited.

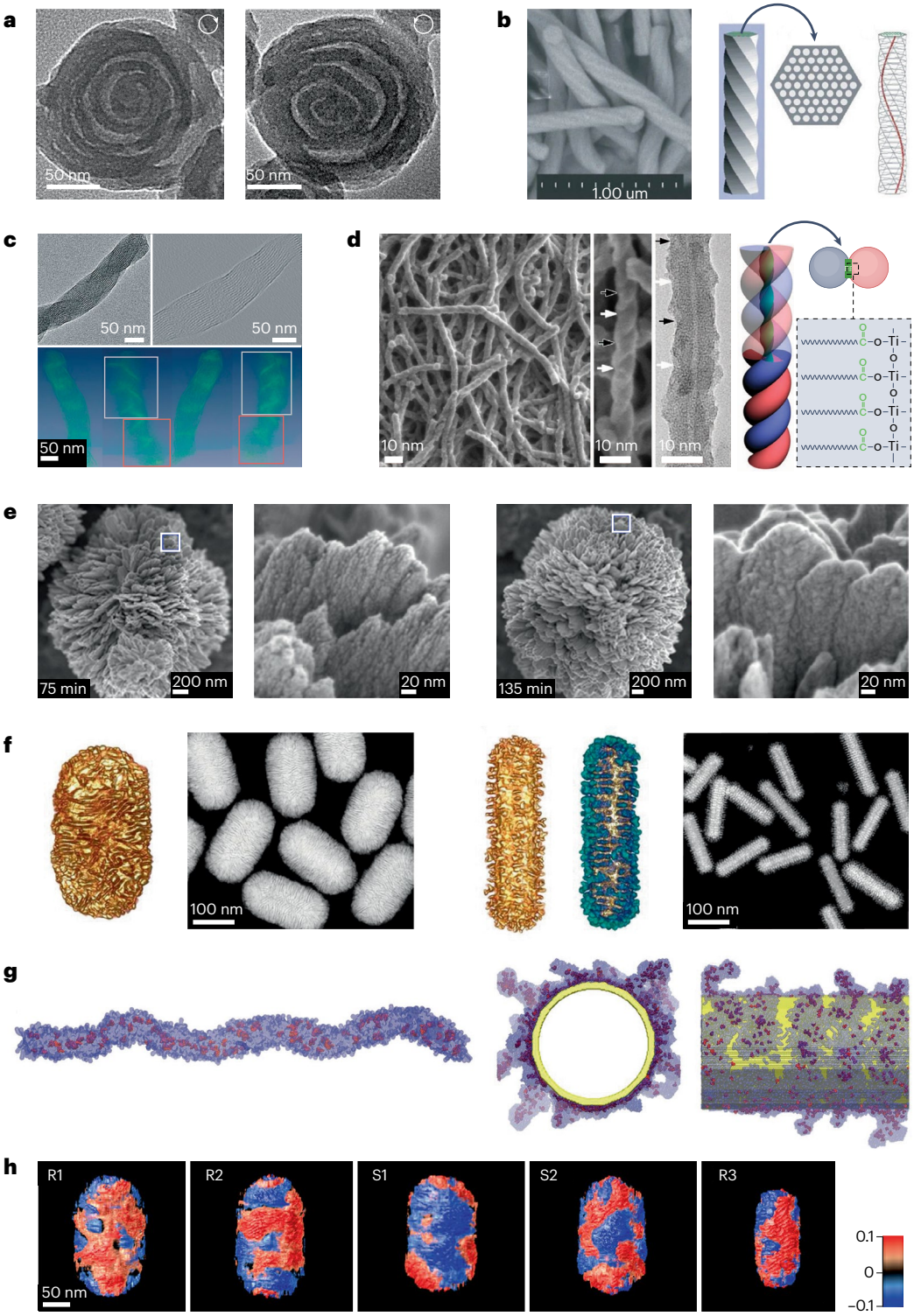

helicoid morphology, these synthesized nanoparticles are called the 432 helicoid series. The synthesis method benefits from straightforward synthetic modifications through change of seed morphologies, chiral biomolecules and the synthetic environment[133–139]. In particular, the 432 helicoid III nanoparticles, synthesized using {111} enclosed octahedron seed nanoparticles and glutathione molecules, have a chiral morphology with four highly curved gaps in a pinwheel-like chiral motif (Fig. 2e). Therefore, the 432 helicoid III particles show strongly biased absorption of CPL, which is attributed to their high-order plasmonic modes[133]. This synthetic platform can also be extended

Fig. 3 | Chiral inorganic nanomaterials synthesized by templating of worm-like helical micelles. a, Transmission electron microscopy (TEM) images of chiral mesoporous carbon nanospheres with right and left-handedness, prepared with spiral micelles[149]. **b**, Scanning electron microscopy (SEM) image and schematics of a structural model of chiral mesoporous silica nanoparticles[151]. **c**, TEM image (top left), central slice through the TEM tomography reconstruction (top right) and voxel projections of the reconstructed volume (bottom) of a chiral silica nanoparticle[153]. **d**, SEM images (scale bars = 100 and 50 nm) of right-handed surfactant–TiO_2 fibres. TEM image (scale bar = 10 nm) (centre) shows a tube in the centre of the fibre, and the schematic shows a structural model of the surfactant–TiO_2 fibre[155]. **e**, SEM images of chiral CuO nanoflowers at different synthesis times, t = 75 min (top left) and 135 min (top right), and their chiral corresponding nanopetals (bottom)[156]. **f**, Tomography reconstruction based on a tilt series of high-angle annular dark-field scanning transmission electron microscopy (HAADF-STEM) images (top left) and a HAADF-STEM projection image (top right) (scale bar, 100 nm) of gold nanorods grown in the presence of chiral micelles; HAADF-STEM (bottom left) and energy dispersive X-ray spectroscopy (bottom centre, platinum displayed in green) tomography reconstruction and HAADF-STEM projection image (bottom right) (scale bar, 100 nm) of chiral gold nanorods coated with platinum[160]. **g**, Molecular dynamics simulations of helical micelles in solution (top); here, aggregation of surfactant (blue) in the presence of co-surfactant (red) results in chiral, worm-like micelles; molecular dynamics simulations for helical micelles adsorbed onto a gold nanorod in axial and lateral views (bottom)[160]. **h**, 3D colour-coded volume renderings of helicity maps for different chiral gold nanorods (red and blue indicate right and left-handed helical features, respectively) (scale bar = 50 nm)[161]. Part **a** reprinted from ref. 149, CC BY 4.0 (https://creativecommons.org/licenses/by/4.0/). Part **b** reprinted from ref. 151, Springer Nature Limited. Part **c** reprinted with permission from ref. 153, Wiley. Part **d** reprinted from ref. 155, Springer Nature Limited. Part **e** reprinted (adapted) with permission from Duan, Y. et al. Optically active chiral CuO "nanoflowers." *J. Am. Chem. Soc.* **136**, 7193–7196 (2014). Copyright 2014 American Chemical Society. Parts **f** and **g** adapted/reprinted from González-Rubio, G. et al. Micelle-directed chiral seeded growth on anisotropic gold nanocrystals. *Science* **368**, 1472–1477 (2020). ©The Authors, some rights reserved; exclusive licensee AAAS. Part **h** is reprinted from ref. 161, CC BY 4.0 (https://creativecommons.org/licenses/by/4.0/).

to other materials, for example, for the synthesis of chiral palladium nanoparticles. Introducing cysteine molecules to palladium nanoparticle synthesis induces spiral structures on each face of the cubic nanoparticles, leading to rotational direction preference with respect to the handedness of the incorporated cysteine molecules[139].

Template-induced synthesis

Biological membranes are based on the ability of surfactants to form micelles in aqueous solution and their tendency to adsorb at interfaces[140], the same as lipids[141]. Amphiphilic molecules can also serve as templates for the structural design of inorganic nanomaterials[142]. By incorporating asymmetric carbon atoms in the chemical structure of surfactants[143], helical micelles can be formed under specific physicochemical conditions (for example, concentration, temperature and ionic strength)[144]. Similarly, dissymmetric nanomaterials can be based on templates made of self-assembled chiral surfactants[145]. However, the availability of chiral surfactants remains limited owing to time-consuming synthesis protocols. Alternatively, commercially available chiral additives can be applied as co-surfactants to induce and tailor helicity in mixed micellar aggregates[146]. Chiral molecules may not be indispensable to the synthesis of chiral inorganic nanomaterials[147]. Self-assembly into spiral micelles can also be induced using conventional surfactants; for example, in molecularly crowded environments[148], helical structures can emerge in chiral multi-shelled mesoporous carbon nanospheres with different morphologies by introducing shear flows and by adjusting the concentration and amphiphilic character of surfactants, that is, by controlling the packing parameters[149] (Fig. 3a).

Mineralization of chiral micelles into chiral silica nanostructures results in a range of morphological features with controlled size, shape, chiral structure and helical pitch length[150]. This synthetic process is based on tuning the interactions at the micelle head group between a chiral anionic amino acid-based surfactant, mixed with the corresponding amino acid precursor as co-surfactant, and a small amount of silica precursors, such as cationic quaternized aminosilanes and tetraethoxylsilane derivatives, under acidic conditions[151]. The presence of helical micelles induces changes in the isotropic condensation and growth of mesoporous silica, thereby leading to a chiral distortion of the final rod-like nanoparticles (Fig. 3b). The resulting morphologies can be simulated by a structural model of twisted shaped rods with inner chiral channels that perfectly match the surfactant micelle organization (Fig. 3b). In addition, the combination of tartrate-based chiral anionic counter-ions, together with achiral ammonium-type surfactants, can direct the handedness of helical silica. Chiral mesoporous silica nanoparticles can also be obtained using fully achiral cationic alkyltrimethylammonium surfactants as templates[152] and tetraethoxylsilane in highly concentrated solutions of ammonia[153]. This process relies on an entropically driven model[154], in which non-chiral micelles take on a helical conformation as a consequence of strong repulsion between ammonium cations and positively charged surfactant head groups, inducing the formation of spiral silica nanoparticle morphologies with helical mesoporous channels (Fig. 3c).

Chirality can also be templated into metal oxide nanomaterials using superstructures of small molecules. For example, crystalline chiral TiO_2 fibres can be synthesized by transcription and calcination of the helical structure formed by anionic amino acid-derived surfactant aggregates, combined with metal–organic titanium precursors[155] (Fig. 3d). Here, chirality transfer is achieved owing to the favourable interaction between the hydrolysed titanium salt and the anionic head groups of the chiral surfactant under acidic conditions, which induces the formation of TiO_2 double helical ribbons with inner tubes (Fig. 3d). Alternatively, achiral anionic surfactants (for example, sodium dodecylsulfate) can serve as structure-directing agents to synthesize chiral CuO flower-like structures using an amino alcohol as the symmetry-breaking co-surfactant, under hydrothermal conditions[156] (Fig. 3e). Such microstructures are composed of nanopetals, in which layers of CuO are stacked and connected into a helical arrangement. Consequently, enantiomeric CuO microflowers with nanopetals of the opposite handedness can be synthesized in the presence of different amino alcohol enantiomers[157].

The cationic surfactant cetyltrimethylammonium bromide (CTAB) can assist the seed-mediated growth of anisotropic gold nanostructures, such as nanorods[158]. In addition, long alcohol chains can be used as co-surfactants to control the organization at the nanoparticle–solvent interface, thereby improving reproducibility in the synthesis of highly monodisperse gold nanorods[159]. Such surfactant-assisted growth allows the engineering of chiral gold nanorods by relying on the templating effect of chiral micelles induced by the presence of an amino-aromatic co-surfactant with axial dissymmetry[160] (Fig. 3f). Molecular dynamics simulations revealed that chiral additives induce

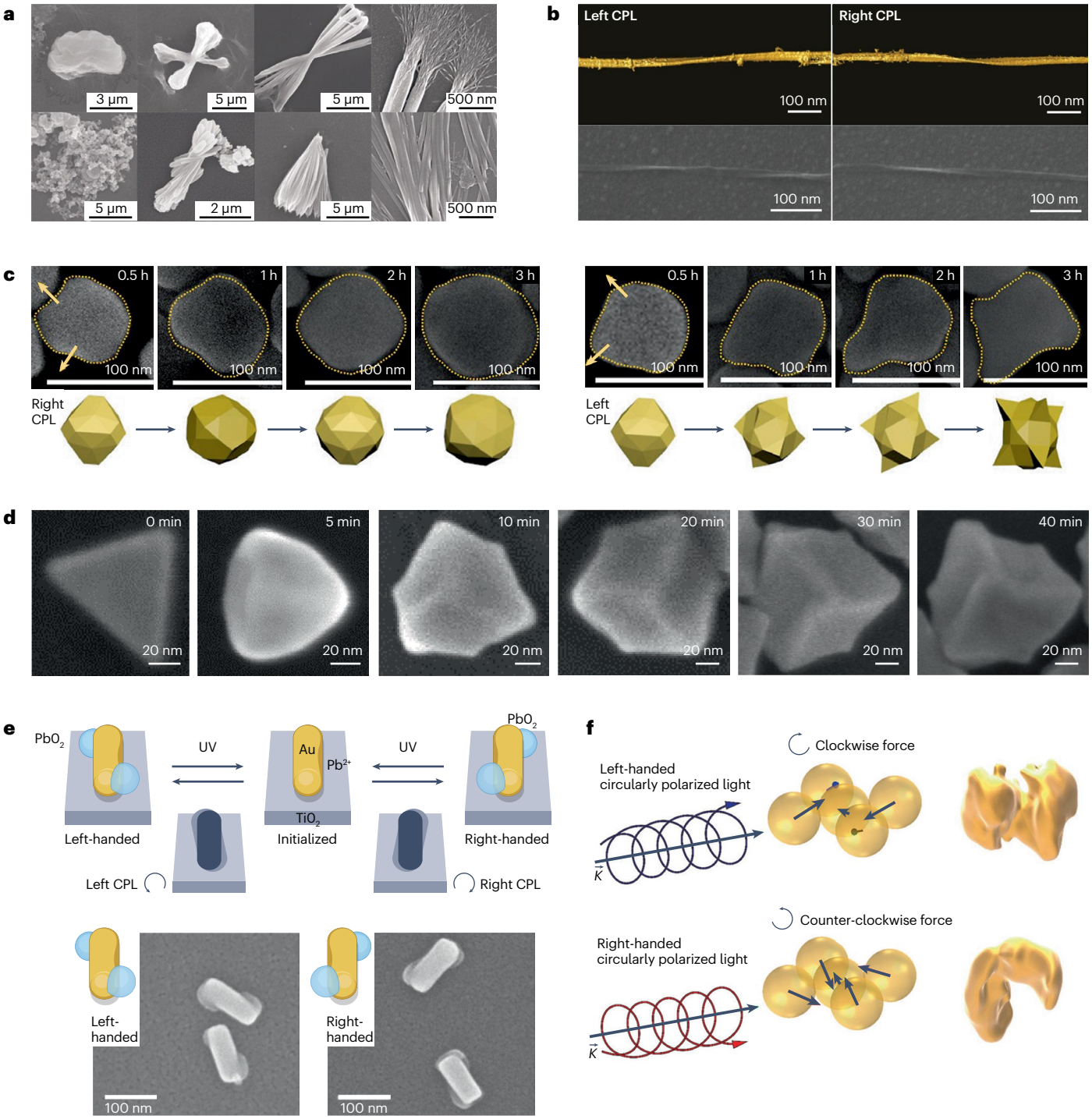

the self-assembly of surfactants into chiral worm-like micelles, which tend to coil around gold nanorods, acting as templates for the seeded growth of chiral features (Fig. 3f). High-angle annular dark-field scanning transmission electron microscopy (HAADF-STEM) tomography reconstructions of such chiral nanorods further demonstrate the presence of sharp wrinkles oriented in a radial direction, displaying tilt angles with respect to the transverse dimension. The resulting chiral templating effect, in which the enantioselective adsorption of micelles at high Miller index surfaces of gold nanorods cannot be excluded, represents an example of the combination of two concomitant chirality generation mechanisms. Interestingly, this approach also works for the synthesis of quasi-helical platinum shells on gold nanorods, as illustrated by HAADF-STEM and energy dispersive X-ray spectroscopy tomography reconstructions (Fig. 3f). The helical

Fig. 4 | Photon and external field-induced chiral nanostructures. a, Formation of chiral cadmium tellutide (CdTe) nanostructures with light (top) and in the dark (bottom) over 72 h. Particles exposed to light form twisted ribbons, whereas particles in the dark form straight ribbons[167]. **b**, Tomographic (top) and scanning electron microscopy (SEM) (bottom) images of CdTe nanoribbons with chirality induced by illumination of left circularly polarized light (CPL) and right CPL. Scale bars = 100 nm (ref. 169). **c**, Growth of chiral gold nanoparticles synthesized with L-cysteine under right and left CPL. Illumination with left CPL amplifies asymmetry, whereas illumination with right CPL reduces assymetry[170]. **d**, SEM images of particles made of gold nanoprisms and L-cysteine–phenylalanine (CYP) dipeptides, and illuminated with left CPL over time. Blade-like structures grow in a spiral shape from the prism surface[173]. **e**, Plasmonic nanostructures with a gold core, deposited with PbO_2 under irradiation with left and right CPL, form chiral particles. PbO_2 can be reduced under UV light. SEM images show chiral (left-handed and right-handed) Au–PbO_2 nanostructures. Scale bars = 100 nm (refs. 175,176). **f**, A solution of gold(III) chloride and citrate illuminated with left or right CPL forms nanostructures with non-obvious chirality[178]. Part **a** adapted/reprinted from Srivastava, S. et al. Light-controlled self-assembly of semiconductor nanoparticles into twisted ribbons. *Science* **327**, 1355–1359 (2010). ©The Authors, some rights reserved; exclusive licensee AAAS. Part **b** adapted from ref. 169, Springer Nature Limited. Part **c** reprinted (adapted) with permission from Wang, H. et al. Selectively regulating the chiral morphology of amino acid-assisted chiral gold nanoparticles with circularly polarized light. *ACS Appl. Mater. Interfaces* **14**, 3559–3567 (2022). Copyright 2022 American Chemical Society. Part **d** reprinted from ref. 173, Springer Nature Limited. Part **e** reprinted (adapted) with permission from Morisawa, K., Ishida, T. & Tatsuma, T. Photoinduced chirality switching of metal-inorganic plasmonic nanostructures. *ACS Nano* **14**, 3603–3609 (2020). Copyright 2020 American Chemical Society. Part **e** reprinted (adapted) with permission from Saito, K. & Tatsuma, T. Chiral plasmonic nanostructures fabricated by circularly polarized light. *Nano Lett.* **18**, 3209–3212 (2018). Copyright 2018 American Chemical Society. Part **f** reprinted (adapted) with permission from Kim, J.-Y. et al. Assembly of gold nanoparticles into chiral superstructures driven by circularly polarized light. *J. Am. Chem. Soc.* **141**, 11739–11744 (2019). Copyright 2019 American Chemical Society.

features in the final chiral nanoparticles can be quantified by analysing their geometrical features, based on electron tomography reconstructions of the gold nanorods (Fig. 3f), allowing the extraction of different parameters, including the inclination angle[161]. This template-induced synthesis approach may be further investigated by exploring new surfactants (for example, gemini surfactants[162]) and biological co-surfactants (for example, amyloid proteins[163]), to obtain metal nanoparticles in which the helical morphology of wrinkles is better defined, and parameters, such as width, depth and pitch, are finely controlled.

Photon-induced chirality in nanomaterials

Light is a desirable source of chirality for the large-scale synthesis of molecular, nanostructured and microstructured materials because of its nearly perfect enantiopurity that is difficult to attain for chemical molecules, even after multiple cycles of purification[164,165]. Additional advantages of CPL as a chirality inducer are the low cost of its mirror asymmetry and the simplicity of spectral tunability[166]. For example, chiral CdTe nanoparticles, prepared with thioglycolic acid (TGA), can be exposed to CPL, which causes photo-oxidation of Te^{2-} and CdS, ultimately driving the replacement of Te^{2-} with S^{2-} ions and self-assembly of the nanoparticles into twisted ribbons[167,168] (Fig. 4a). Enantiomeric excess exceeding 30% can be achieved by illumination of twisted nanoribbons with left and right-handed CPL, resulting in twisted nanoribbons with identical handedness[169] (Fig. 4b). CPL irradiation drives the ion exchange of Te^{2-} with S^{2-} through TGA photo-oxidation. Owing to the chiral geometry of the individual nanoparticles, one enantiomer in the racemic mixture preferentially absorbs chiral light of the same handedness, resulting in the formation of nanoribbons made primarily of one 'nano-enantiomer'[169]. CPL can also be used to alter the shape of chiral materials, by either increasing or reducing their asymmetry. Chiral nanoparticles made of gold, grown with left-handed or right-handed CPL, become more asymmetric when illuminated with light of the same handedness as the particle, and less asymmetric when illuminated with light of the opposite handedness[170] (Fig. 4c).

Correspondingly, asymmetry can also be introduced into achiral shapes using CPL. Achiral gold nanoprisms made in the presence of chiral dipeptides can be grown into chiral particles under CPL. Here, light generates localized electric field hot spots, which tend to form at the edges and vertices of anisotropic plasmonic nanoparticles[101,171,172]. Under exposure to CPL, blade-like protrusions are formed at the nanoprism core, which further grow into a spiral pattern through the generation of hot spots at the nanoparticle corners (Fig. 4d). Although the handedness of the resulting particles originates from the dipeptide used in the synthesis, the extent of asymmetry in the resulting nanoparticles can be adjusted through the use of either left-handed CPL, right-handed CPL or linearly polarized light[173]. Chiral nanostructures can also be created using plasmon-induced charge separation, to grow a chiral shape from an achiral core without the addition of chiral molecules or nanoparticles[166,174]. For example, CPL can create chiral particles from colloidal gold nanocuboids and lead nitrate. Here, the incident light is circularly polarized, causing the formation of hot spots on specific corners of the gold cuboid cores, where growth is then driven through the oxidation of Pb^{2+} into PbO_2. As a result, the nanoparticles acquire a chiral shape without the addition of chiral molecules[166]. This process can be reversed by reduction of PbO_2 with UV light, resulting in a soluble form separated from the gold core. Therefore, the handedness and morphology of the particles can be modulated using light only[175,176] (Fig. 4e). Computational modelling suggests that chiral structures synthesized with CPL can be smaller than their resonant wavelength, and that gold nanoparticles can be grown into homogeneous chiral particles by depositing gold through a chemical reaction driven by the hot spots[177]. Moreover, CPL can be used to grow chiral nanoparticles directly from metal ions in solution. In an achiral solution of gold chloride hydrate and citrate ions, CPL leads to a chemical reduction chiral nanoparticles. This light to matter chirality transfer has high efficiency for gold, with enantiomeric excess exceeding 30%[178]. The resulting particles are non-helical and non-tetrahedral, and thus their handedness can be determined by calculating their Osipov–Pickup–Dunmur chirality descriptor, which measures the change in positive to negative sign, when a chiral geometrical structure is reflected in a mirror[178] (Fig. 4f).

Applications

The diversity of synthesis procedures and resulting properties of chiral nanostructures allow various applications, including photonics, sensing, catalysis, drug delivery and biomedicine. Although primarily explored for photonics and sensing thus far, bioinspired chiral inorganic nanomaterials may be applied for various other applications, including in biomedicine (Fig. 5).

Photonics

Chiral materials differently absorb left-handed and right-handed CPL. Their chiroptical properties can be described by their *g*-factor, which refers to the dimensionless ratio of circular dichroism to extinction at any given wavelength. This ability to selectively absorb chiral light renders chiral particles particularly useful for photonics[179]. Materials with a high *g*-factor, and thus high chiroptical activity, can efficiently modulate the polarization of light. For example, the 432 helicoid III nanoparticles provide control over the polarization state of light, exhibiting a maximum *g*-factor of 0.2. By altering the size of these particles, through varying the initial concentration of seed nanoparticles, the wavelength displaying the maximum *g*-factor can be finely tuned. Under cross-polarized conditions and using different angles of an analyser filter, particles with different sizes enable precise modulation of visible light, generating vivid colours[133]. Of note, the non-linear optical response of chiral nanomaterials may be stronger than the linear response; for example, 432 helicoid III nanoparticles have non-linear *g*-factors of up to −1.63 (ref. 180). The strong and tunable scattering of these particles make them applicable in photonic systems, such as emitters[180].

Other non-linear optical responses in chiral nanostructures include third harmonic Mie scattering on CdTe helices dispersed in liquid. Studies of the non-linear optical effects of these helices have resulted in the discovery of a new method to characterize the chiroptical properties of nanomaterials with sample volumes of less than 1 µl, which is a hundred to a thousand times smaller than what is currently required[181,182]. Micelle-directed chiral growth on gold nanorods results in materials with intense circular dichroism, which can be tuned by adjusting the seed conditions, such as the concentration of gold nanorod seeds in the growth solution. Here, the optical activity can be readily extended into the near-infrared (NIR) range, even reaching telecommunication wavelengths[160].

Sensing

The optical activity of chiral materials can also be exploited for (bio) sensing, based on changes in the peak wavelength of the circular dichroism signal[183]. Chiral gold or silver nanoparticles selectively aggregate in the presence of one of the enantiomers of a small molecule, thereby resulting in a colour change of the colloid[184–186]. Gold nanoparticles can also be used in conjunction with cysteine-modified nanoparticles for the detection of L- or D-cysteine. The NIR light emission of the gold nanorod–nanoparticle system is quenched in the presence of cysteine of the same enantiomer as the nanoparticle. However, such systems need to be tailored for specific analytes, limiting their versatility[187].

Chiral plasmonic nanostructures, including gold, silver, magnesium and alloyed materials, can be applied for chemical sensing by exploiting their localized surface plasmon resonances[188–190]. Chiral plasmonic nanostructures greatly improve the limit of (bio)molecule detection based on circular dichroism spectroscopy, compared with

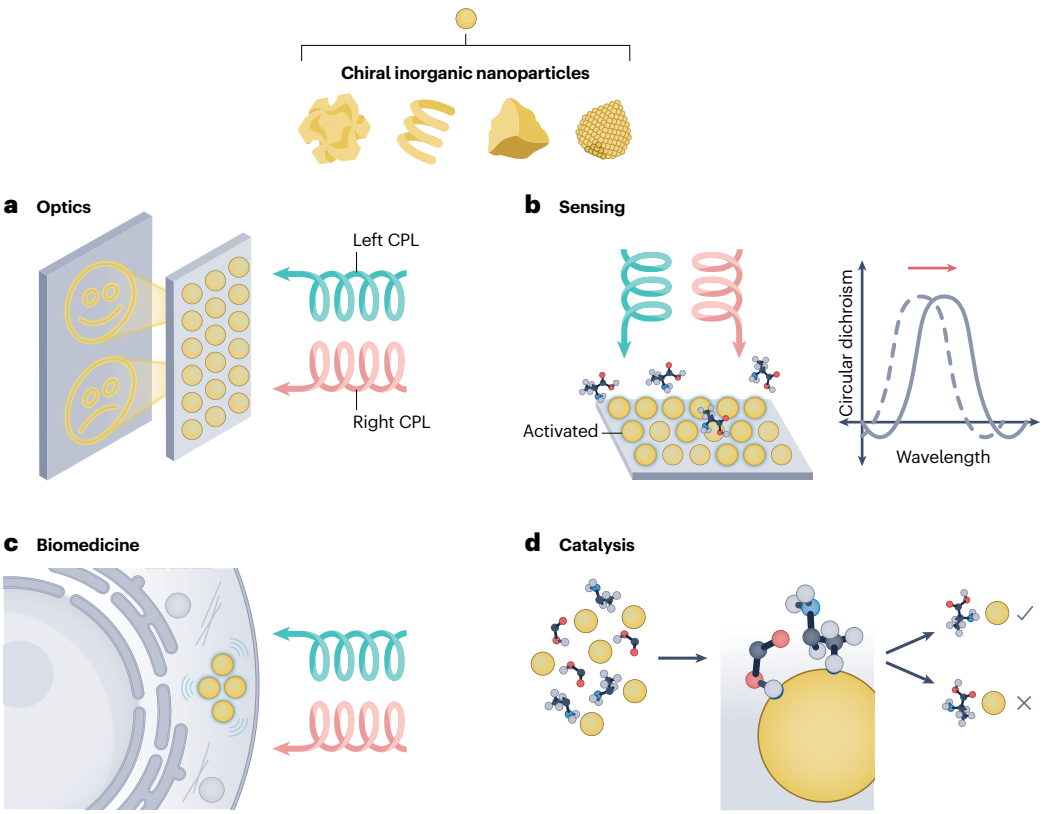

Fig. 5 | Applications of bioinspired chiral inorganic nanomaterials. The diversity of synthesis procedures and resulting properties of chiral nanostructures may allow applications with respect to the design of chiral nanomaterials. **a**, In photonics, selective modulation of optical responses can be achieved by exploiting the chirality of nanomaterials. **b**, In sensing, chiral nanomaterials enable the highly sensitive detection of molecular chirality. **c**, In biomedicine, the handedness-specific impact of chiral nanomaterials on cells and the cellular environment can be exploited for modulating cells and cellular components. **d**, In catalysis, selective synthesis of chiral molecules can be achieved using chiral nanomaterials. CPL, circularly polarized light.

colorimetric probes[191], because nanoscale particles have a markedly different distance dependence for polarization rotation compared with absorption, and because plasmonic nanoparticles typically have low-noise circular dichroism spectra in the 500–800 nm spectral window[192]. Subtle changes in the local refractive index may induce a localized surface plasmon resonance shift[193]. For example, the hydrogenation of palladium nanohelices decreases the intensity of the circular dichroism signal, allowing the optical detection of hydrogen gas concentration in air[189]. Chiral assemblies comprising a gold shell as a core made of gold nanoparticle satellites (linked through DNA hybridization) can detect the presence of the mycotoxin ochratoxin A through changes in the intensity of the circular dichroism signal[194]. Gold nanorod assemblies have been used to detect attomolar levels of DNA through a polymerase chain reaction-based assembly method[195]. The initial concentration of DNA alters the circular dichroism signal intensity of the nanorod assemblies, and these changes can be used to determine the presence and concentration of DNA segments[196].

Circular differential scanning intensity spectra can be recorded for single particles. By averaging multiple circular differential scanning intensity measurements over time, contributions to the circular differential scanning intensity from linear optical anisotropies approach zero. The ability to detect a chiroptical signal from a single plasmonic nanoparticle paves the way for the development of new types of plasmonic sensing[195]. Plasmonic sensors with chiral inorganic morphologies are typically synthesized by top-down approaches, such as lithography, which often require expensive, specialized equipment[183,197]. By limiting batch to batch variation between particles, chiral sensors could be produced with high throughput and low costs[198].

Catalysis

The biomimetic and bioinspired aspects of chiral nanoparticles can be particularly attractive in chiral catalysis occurring on chiral supraparticle assemblies that replicate (in size, function and formation pathway) similar organelles in bacteria. Chiral assemblies of ZnS nanoparticles, stabilized with L- or D-penicillamine, catalyse the photooxidation of tyrosine, with preference for the same handedness as that in the nanoparticle assembly. Coupling between the different nanoparticles in the assembly induces the transfer of excited states, while protecting the ligands near the core of the assembly, thereby improving the stability of the chiral catalyst[199]. Chiral selectivity in inorganic nanomaterials originates from the combination of chiral atomic surfaces and a strong chiroptic response. Furthermore, nanostructured assemblies with macroscopic chiral morphologies often possess chiral atomic sites that can enantiospecifically interact with chiral molecules. For example, cysteine-induced chirality of gold nanoparticles has precise homochiral facets, which can selectively catalyse the electrooxidation of L- and D-tryptophan[200]. During electro-oxidation, chiral gold nanoparticles with $\{12\ \bar{5}\ 8\}^{R}$ facets promote a higher oxidation current density for L-tryptophan than for D-tryptophan. Similarly, chiral cavities generated by L- and D-3,4-dihydroxyphenylalanine on mesoporous metal structures can enantioselectively distinguish chiral molecules[201]. The chiral cavities serve as active sites and retain their chiral character even after removal of the molecular template. This approach can be applied for enantioselective catalysis, for example, for the electrochemical reduction of achiral phenylglycolic acid into chiral mandelic acid[202].

The optical activity of chiral metal nanoparticles dictates the directionality of catalysis[203]. Chiral gold nanoparticle cores impart chirality dependence to the photocatalytic properties of achiral shell materials. Particles with a CdS shell show increased hydrogen evolution when illuminated with light of handedness matching that of the particle, compared with the opposite chirality or the use of linearly polarized light[204]. Metallic nanohelices, made from silver or copper, enantioselectively catalyse the photocyclodimerization of anthracene-2-carboxylic acid, as a result of chiroplasmonic effects at the nanohelix surface[204,205].

Furthermore, chiral nanoparticles can selectively cleave DNA. CdTe nanoparticles with chiral ligands recognize and cut a specific restriction site through photonic excitation. Particles illuminated with CPL of the opposite chirality produce reactive oxygen species (ROS), including hydroxyl radicals, which oxidize the phosphodiester bond between the T and A bases in DNA. Although the efficiency of this reaction does not depend on the enantiomer of the cysteine ligand, chirality is important because the production of ROS is affected by the relative handedness of the incident light and the ligand[206]. Similarly, cysteine-derived, chiral carbon dots may cleave single strands of a DNA double helix by producing hydroxyl radicals. Here, the biomimetic enzyme-like function of the chiral carbon dots is realized through stronger intercalative binding of D-cysteine to DNA, compared with L-cysteine, making carbon dots synthesized with D-cysteine more efficient catalysts[207].

Biomedical applications

In biomedical applications, NIR wavelengths are preferred because of their longer penetration depth through tissues[208]. For example, CdTe helices have tunable optical activities in NIR wavelengths, and can thus be used to modulate light for biomedical and optical computing applications[181]. Chiral molybdenum oxide nanoparticles can be applied for photothermal therapy, increasing light-induced heating under CPL. The strong absorption of these particles allows local heating of tumour tissue, without causing radiation damage to healthy tissue[209]. Gold nanobipyramids conjugated with D-Glu show enhanced bactericidal effects, compared with achiral nanoparticles or L-Glu, through the synergistic effect of multiple mechanisms, although the exact mechanisms remain to be elucidated. D-Glu can inhibit D-Glu-associated catalysis, thereby disrupting peptidoglycan biosynthesis, which is crucial for bacterial cell wall viability. In addition, physical piercing of gold nanobipyramids into the bacterial cell wall promotes leakage, further enhancing the antibacterial effect. Moreover, under NIR radiation, photothermal heating of gold nanobipyramids decreases the viability of *Staphylococcus epidermidis*, promoting healing in infected rat wounds[210].

The intrinsic structural chirality of gold nanomaterials can also be exploited to modulate the immune system[173]. For example, achiral and left-handed and right-handed gold biomimetic nanoparticles elicit different immune responses in vitro and in vivo. Importantly, the intrinsic structural chirality of the nanoparticles is triggering the immune response. Binding of nanoparticles to the G-protein-coupled receptors cluster of differentiation 97 (CD97) and epidermal growth factor-like module receptor 1 (EMR1) results in endocytosis of the nanoparticle and the opening of mechanosensitive potassium-efflux channels, causing the production of inflammasomes. Although both enantiomers undergo endocytosis, the left-handed nanoparticle enantiomer shows stronger association with the receptors owing to supramolecular interactions between the curved chiral nanoparticle surface and the chiral extracellular domains (epidermal growth factor (EGF)-like segments) in both receptors. Selective blocking of the potassium-efflux channels inhibits inflammasome activation, indicating the importance of these channels in the immune response to the gold nanoparticles. Therefore, chiral nanoparticles have been explored as adjuvants for the H9N2

influenza vaccine in C57BL/6 mice. Here, left-handed nanoparticles showed 1,258-fold higher influenza-specific antibody generation, compared with right-handed nanoparticles, along with an increase of immune-related cell proliferation. Such enantiomer-dependent immune reactivity of engineered chiral inorganic nanostructures raises the possibility of immune response modulation through nanomaterials, highlighting the important role of nanoscale chirality in biological systems, in addition to the molecular (angstrom) scale chirality of L/D optical centres.

Outlook

Chiral inorganic nanomaterials may be applied for various biomedical and bioengineering applications, such as sensing, photothermal and photodynamic cancer therapy, and neurodegenerative disease therapy[211]. The handedness-dependent physicochemical properties of chiral inorganic nanomaterials can be exploited to modulate biological components at the nanoscale, such as site-selective biocatalytic activities or immune response activation. However, clinical-level applications are yet to be developed owing to the limited understanding of the interactions between chiral inorganic surfaces and biological environments. Diversification and sophistication of chiral inorganic surfaces will increase our understanding of organic–inorganic interface dynamics and play a crucial role in their translation for biomedical applications. Chiral gold nanoparticles can manipulate immune signalling by enantiomer-dependant receptor interaction with respect to their *g*-factor, which is directly correlated to structural chirality[173], indicating that further structural complexity in chiral nanomaterials may diversify organic–inorganic interactions to expand their applicability in biomedical applications, such as cancer immunotherapy, by modulating immune cell dynamics to alter the cancer immunity cycle[212].

In enantioselective biosensing, the systematic assembly of individual chiral inorganic nanomaterials could substantially improve sensitivity and, thus, practical implementation. For example, enantioselective sensing could be achieved using freely dispersed 3D chiral inorganic nanomaterials and lithographed plasmonic structures in preclinical demonstrations to monitor avidin binding events or identify virus structures[193,213]. In particular, ensemble averaging of analyte detection and measurements at different relative orientations and positions[102] would improve sensitivity and measurement robustness in biosensing. This could be achieved using unidirectional optical chirality induced by oriented assembly, or lattice structures made of individual chiral inorganic nanostructures[214].

Importantly, exposure of chiral inorganic nanomaterials to a biological environment opens up the possibility of using handedness-dependent organic–inorganic interactions between chiral surfaces of nanomaterials and chiral molecules, so that the inorganic surface geometry may recognize conformational differences in adsorbed biological entities for target-specific biochemistry and molecular sensing. To control the interaction dynamics at the nanoscale or sub-nanoscale level, precise nanostructure surfaces are required. Therefore, characterization methods need to be optimized to precisely quantify and understand the structural chirality of individual nanomaterials, going beyond circular dichroism and electron microscopy. Although these optical and morphological analyses provide some level of understanding of the chiral system, the detailed construction and evolution mechanism of chirality may not be fully assessable. The following characterization methods may serve as analytical techniques to enumerate the mechanistic complexity of chiral inorganic nanomaterials.

Tomographic and crystallographic analysis

3D characterization tools can be used to analyse nanoparticle morphologies[161,215–217]. For example, the 3D helical morphology of gold nanorods can be analysed using electron tomography reconstructions at a single-nanoparticle level. However, the interpretation of such 3D reconstructions remains challenging and mainly relies on visual inspection. Alternatively, 3D Fourier transformations of electron tomography reconstructions allow the identification of chiral features on nanorods; however, this approach cannot provide quantitative data representative of nanorod chirality[160], which would be required to gain better insight into the relation of surface morphology and chiroptic response. In addition, traditional chirality assessments, such as the Hausdorff distance and Osipov–Pickup–Dunmur chirality, can be applied for the 3D reconstruction of gold nanostructures[178]; through decomposing electron tomography reconstructions of a chiral shape into a combination of helices[161], helical features can be spatially resolved and quantitative parameters can be extracted that can be related to chiral geometry. However, 3D reconstructions of nanostructures can take time because the computational alignment and reconstruction can take hours to days. Alternatively, acquisition and processing of data from transmission electron microscopy (TEM) tomography enables real-time 3D tomographic visualization of chiral specimens in real time, as data are collected in an electron microscope. Volumetric interpretation and calculation of chirality measures can begin in less than 10 min and a high-quality tomogram can be available within 30 min, as demonstrated for twisted bowtie assemblies[218]. Here, the calculation of chirality should be incorporated into the tomography software, including the open source package tomviz.

Crystallography allows the definition of exposed facets of chiral nanoparticles to assess their evolutionary pathways. For example, all possible surface orientations, including chiral surfaces, could be defined using the stereographic projection of the face-centred cubic lattice, allowing the assessment of exposed chiral surfaces in synthesized nanoparticles and analysis of their growth trajectories[137]. 3D characterization of the surface structure at an atomic scale would further give insight into the exact nature of chiral surfaces and micro-facets. Although atomic resolution electron tomography is possible[219,220], a reliable analysis of surface facets remains challenging owing to potential artefacts, for example those related to the limited tilt range[221] during acquisition. Improvement of the acquisition of tilt series and reconstruction algorithms for electron tomography might overcome such limitations[222,223].

Surface-sensitive techniques in TEM, such as secondary electron imaging in scanning TEM, could reveal the presence and role of chiral facets during growth[224]. However, imaging surface molecules remains difficult because of their lack of contrast and sensitivity to the electron beam. Advanced TEM techniques, such as exit wave reconstruction, allow the visualization of hard–soft matter interfaces, for example metal–polymer heterojunctions[225]. This technique may also be applied for 3D characterization, for example, to allow direct visualization of shape-directing additives at the surface of metal nanoparticles.

Single-nanoparticle optical analysis

Single nanoparticle-level analysis of the optical response of chiral inorganic nanomaterials is crucial for the accurate quantification of chirality. Ensemble observation provides a quick and qualitative understanding of chiral systems; however, it relies on averaging the optical activity of individual chiral nanostructures. To correlate the optical spectrum of individual chiral nanostructures with their morphologies,

modified dark-field transmission microscopy and single-particle chiral scatterometry can be used. These techniques can better detect the optical properties of chiral nanostructures, compared with ensemble measurements. Importantly, slight structural differences in individual chiral structures may cause large deviations in the optical spectra, hindering average ensemble optical responses[226,227]. Based on such measurements, a design principle has been proposed with modified synthetic conditions to construct chiral nanostructures with uniform chiral features, which allowed a significant enhancement of the *g*-factor from 0.2 to 0.3 (ref. 134) and 0.4 (ref. 173). Furthermore, single particle-level analysis would improve our understanding of nanomaterials dynamics in a biological environment, as well as interaction mechanisms at the molecular and nanoscale. For example, nanoparticle interactions in the body can be represented by the lock and key interaction model to analyse the effect of nanoparticle morphology and chirality on the dynamics of targeting ligand–receptor interactions, such as in immune bone marrow cells and cancer cell membranes. Single-nanoparticle orientation studies[228] and multiscale structural descriptors[229] can be applied to assess such lock and key interactions. Single nanoparticle-level observations of nanocatalysts have also provided insight into catalytic mechanisms[230]. Therefore, single nanoparticle-level analysis may improve our understanding of enantioselective interactions at the organic–inorganic interface, and the functionality of chiral inorganic nanomaterials in biological environments.

Mathematical structure and pattern analysis

New theoretical models are required to elucidate chirality transfer mechanisms and the role of chirality in the assembly and functioning of biological structures. Mathematical description and pattern analysis of self-assembled chiral components could enable direct comparison of preparation pathways of materials with nanoscale, microscale and macroscale chiral geometries. Graph theory can be applied to assess the relationship between multiscale chirality, the geometries of self-assembled structures and their functionalities[28,178,231–233], for example to analyse the structural complexity of hierarchically organized assemblies of Au-Cys nanoplatelets[28]. Graph theory is applicable to any scale, thus enabling the quantitative comparison of different chiral morphologies with mirror asymmetry. In addition, an assembly structure phase diagram can be constructed to study the role of particle chirality in different assembly pathways[28]. Importantly, chirality and other aspects of geometry are represented as graphs resembling atomic graphs in chemistry (that is, molecules), which may be directly correlated to properties such as polarization rotation or colloidal stability. The graph theory representations and related complexity index calculations can be used as a guide for the engineering of biomimetic chiral particles and their assemblies. In practice, graph theory enables direct parametrization of atomic and nanoscale geometries, which, in turn, enables the unification of structural descriptors for biological and abiological nanostructures[229]. Combining graph theory descriptors with chirality measures extracted from the protein data bank and electron microscopy images would open the road for the engineering of chiral nanostructures for targeted formation of protein–nanoparticle complexes that mimic protein–protein complexes with lock and key matches of their chirality and concavity. Unified structural descriptors, including chirality measures, may also be used for training machine learning algorithms to accelerate the design of chiral nanoparticles targeting specific proteins, which currently relies on conceptual intuitive guessing or laborious Edisonian processes[234].

Computational modelling

Chiral inducer molecules play an essential role in the chiral growth of crystalline nanomaterials, transferring their chirality to an inorganic lattice that may be distorted. Macro-kinetic modelling of such mechanisms requires knowledge of thermodynamic and kinetic effects of diastereomers and enantiomers. Petascale supercomputers enable computational modelling that integrates density functional theory and molecular dynamics simulations, which may allow the macro-kinetic modelling of chirality transfer processes, ultimately aiming at prediction to improve the synthesis of chiral nanomaterials, taking inspiration from biological systems.

Published online: 27 January 2023

References

1. Bar-Cohen, Y. Biomimetics — using nature to inspire human innovation. *Bioinspir. Biomim.* **1**, P1–P12 (2006).
2. Rus, D. & Tolley, M. T. Design, fabrication and control of soft robots. *Nature* **521**, 467–475 (2015).
3. Mussa-Ivaldi, S. Real brains for real robots. *Nature* **408**, 305–306 (2000).
4. Kalb, C. Leonardo's enduring brilliance. *Natl. Geogr. Mag.* 56–93 (May 2019).
5. Binnig, G., Quate, C. F. & Gerber, C. Atomic force microscope. *Phys. Rev. Lett.* **56**, 930–933 (1986).
6. Garcia, R. & Herruzo, E. T. The emergence of multifrequency force microscopy. *Nat. Nanotechnol.* **7**, 217–226 (**2012**).
7. No authours listed. 'Plenty of room' revisited. *Nat. Nanotechnol.* **4**, 781 (2009).
8. Schliwa, M. & Woehlke, G. Molecular motors. *Nature* **422**, 759–765 (2003).
9. Nicholas, A. K. Self-assembly of inorganic nanoparticles: ab ovo. *Europhys. Lett.* **119**, 66008 (2017).
10. Weiner, S. & Wagner, H. D. The material bone: structure–mechanical function relations. *Annu. Rev. Mater. Sci.* **28**, 271–298 (1998).
11. Seeman, N. C. & Belcher, A. M. Emulating biology: building nanostructures from the bottom up. *Proc. Natl Acad. Sci. USA* **99**, 6451–6455 (2002).
12. Wei, G. et al. Self-assembling peptide and protein amyloids: from structure to tailored function in nanotechnology. *Chem. Soc. Rev.* **46**, 4661–4708 (2017).
13. Badylak, S., Freytes, D. & Gilbert, T. Extracellular matrix as a biological scaffold material: structure and function. *Acta Biomater.* **5**, 1–13 (2009).
14. Kotov, N. A., Meldrum, F. C., Wu, C. & Fendler, J. H. Monoparticulate layer and Langmuir–Blodgett-type multiparticulate layers of size-quantized cadmium sulfide clusters: a colloid-chemical approach to superlattice construction. *J. Phys. Chem.* **98**, 2735–2738 (1994).
15. Ilton, M. et al. The principles of cascading power limits in small, fast biological and engineered systems. *Science* **360**, eaao1082 (2018).
16. Pulido, A. et al. Functional materials discovery using energy–structure–function maps. *Nature* **543**, 657–664 (2017).
17. Kotov, N. A., Dékány, I. & Fendler, J. H. Ultrathin graphite oxide–polyelectrolyte composites prepared by self-assembly: transition between conductive and non-conductive states. *Adv. Mater.* **8**, 637–641 (1996).
18. Whitesides, G. M. & Grzybowski, B. Self-assembly at all scales. *Science* **295**, 2418–2421 (2002).
19. Kotov, N. A., Dekany, I. & Fendler, J. H. Layer-by-layer self-assembly of polyelectrolyte–semiconductor nanoparticle composite films. *J. Phys. Chem.* **99**, 13065–13069 (1995).
20. Whitesides, G. Nanoscience, nanotechnology, and chemistry. *Small* **1**, 172–179 (2005).
21. Guerrero-Martínez, A., Grzelczak, M. & Liz-Marzán, L. M. Molecular thinking for nanoplasmonic design. *ACS Nano* **6**, 3655–3662 (2012).
22. Levin, A. et al. Biomimetic peptide self-assembly for functional materials. *Nat. Rev. Chem.* **4**, 615–634 (2020).
23. Kotov, N. A. (ed.) *Nanoparticle Assemblies and Superstructures* (CRC, 2016).
24. Dzenis, Y. Spinning continuous fibers for nanotechnology. *Science* **304**, 1917–1919 (2004).
25. Gates, B. D. et al. New approaches to nanofabrication: molding, printing, and other techniques. *Chem. Rev.* **105**, 1171–1196 (2005).
26. Huebsch, N. & Mooney, D. J. Inspiration and application in the evolution of biomaterials. *Nature* **462**, 426–432 (2009).
27. Zhang, S. Fabrication of novel biomaterials through molecular self-assembly. *Nat. Biotechnol.* **21**, 1171–1178 (2003).
28. Jiang, W. et al. Emergence of complexity in hierarchically organized chiral particles. *Science* **368**, 642–648 (2020).
29. Kotov, N. A., Meldrum, F. C., Fendler, J. H., Tombacz, E. & Dekany, I. Spreading of clay organocomplexes on aqueous solutions: construction of Langmuir–Blodgett clay organocomplex multilayer films. *Langmuir* **10**, 3797–3804 (1994).
30. Sarikaya, M. Biomimetics: materials fabrication through biology. *Proc. Natl Acad. Sci. USA* **96**, 14183–14185 (1999).

31. Barthelat, F. Biomimetics for next generation materials. *Philos. Trans. R. Soc. A Math. Phys. Eng. Sci.* **365**, 2907–2919 (2007).
32. Mirkin, C. A., Letsinger, R. L., Mucic, R. C. & Storhoff, J. J. A DNA-based method for rationally assembling nanoparticles into macroscopic materials. *Nature* **382**, 607–609 (1996).
33. Buschmann, H., Thede, R. & Heller, D. New developments in the origins of the homochirality of biologically relevant molecules. *Angew. Chem. Int. Ed.* **39**, 4033–4036 (2000).
34. Pasteur, M. L. Recherches sur les relations qui peuvent exister entre la forme cristalline, la composition chimique et les sens de la polarisation rotatoire [French]. *Ann. Chim. Phys* **24**, 442–460 (1848).
35. Thomson, K. & Baron, W. *Baltimore Lectures on Molecular Dynamics and the Wave Theory of Light* (C. J. Clays and Sons, 1904).
36. Guijarro, A. & Yus, M. *The Origin of Chirality in the Molecules of Life* (Royal Society of Chemistry, 2008).
37. Barron, L. D. & Barron, L. D. *Molecular Light Scattering and Optical Activity* (Cambridge Univ. Press, 2004).
38. Guerrero-Martínez, A., Alonso-Gómez, J. L., Auguié, B., Cid, M. M. & Liz-Marzán, L. M. From individual to collective chirality in metal nanoparticles. *Nano Today* **6**, 381–400 (2011).
39. Berova, N., Bari, L., Di & Pescitelli, G. Application of electronic circular dichroism in configurational and conformational analysis of organic compounds. *Chem. Soc. Rev.* **36**, 914 (2007).
40. Kelly, S. & Price, N. The use of circular dichroism in the investigation of protein structure and function. *Curr. Protein Pept. Sci.* **1**, 349–384 (2000).
41. Vukusic, P. Evolutionary photonics with a twist. *Science* **325**, 398–399 (2009).
42. Sharma, V., Crne, M., Park, J. O. & Srinivasarao, M. Structural origin of circularly polarized iridescence in jeweled beetles. *Science* **325**, 449–451 (2009).
This article reports the ability of the scarab beetle to reflect structural colour from its external surfaces in the form of left-handed CPL.
43. Pizzarello, S. & Weber, A. L. Prebiotic amino acids as asymmetric catalysts. *Science* **303**, 1151 (2004).
44. Parker, A. R. & Townley, H. E. Biomimetics of photonic nanostructures. *Nat. Nanotechnol.* **2**, 347–353 (2007).
45. Vukusic, P. & Sambles, J. R. Photonic structures in biology. *Nature* **424**, 852–855 (2003).
46. Chen, W. et al. Nanoparticle superstructures made by polymerase chain reaction: collective interactions of nanoparticles and a new principle for chiral materials. *Nano Lett.* **9**, 2153–2159 (2009).
47. Pendry, J. B. A Chiral route to negative refraction. *Science* **306**, 1353–1355 (2004).
48. Wang, B., Zhou, J., Koschny, T., Kafesaki, M. & Soukoulis, C. M. Chiral metamaterials: simulations and experiments. *J. Opt. A Pure Appl. Opt.* **11**, 114003 (2009).
49. Liu, Y. & Zhang, X. Metamaterials: a new frontier of science and technology. *Chem. Soc. Rev.* **40**, 2494 (2011).
50. Ma, W. et al. Chiral inorganic nanostructures. *Chem. Rev.* **117**, 8041–8093 (2017).
51. Fan, J. & Kotov, N. A. Chiral nanoceramics. *Adv. Mater.* **32**, 1906738 (2020).
52. Lv, J. et al. Self-assembled inorganic chiral superstructures. *Nat. Rev. Chem.* **6**, 125–145 (2022).
53. Ahn, H.-Y. et al. Bioinspired toolkit based on intermolecular encoder toward evolutionary 4D chiral plasmonic materials. *Acc. Chem. Res.* **52**, 2768–2783 (2019).
54. Ozturk, S. F. & Sasselov, D. D. On the origins of life's homochirality: inducing enantiomeric excess with spin-polarized electrons. *Proc. Natl Acad. Sci. USA* **119**, e2204765119 (2022).
55. Kuncha, S. K., Kruparani, S. P. & Sankaranarayanan, R. Chiral checkpoints during protein biosynthesis. *J. Biol. Chem.* **294**, 16535–16548 (2019).
56. Melnikov, S. V. et al. Mechanistic insights into the slow peptide bond formation with D-amino acids in the ribosomal active site. *Nucleic Acids Res.* **47**, 2089–2100 (2019).
57. Fujii, N. N., Takata, T. & Fujii, N. N. Quantitative analysis of isomeric (l-α-, l-β-, d-α-, d-β-) aspartyl residues in proteins from elderly donors. *J. Pharm. Biomed. Anal.* **116**, 25–33 (2015).
58. Sakaue, H., Kinouchi, T., Fujii, N. N., Takata, T. & Fujii, N. N. Isomeric replacement of a single aspartic acid induces a marked change in protein function: the example of ribonuclease A. *ACS Omega* **2**, 260–267 (2017).
59. Abdulbagi, M., Wang, L., Siddig, O., Di, B. & Li, B. D-Amino acids and D-amino acid-containing peptides: potential disease biomarkers and therapeutic targets? *Biomolecules* **11**, 1716 (2021).
60. Nakamura, M. & Hashimoto, T. Mechanistic insights into plant chiral growth. *Symmetry* **12**, 2056 (2020).
61. Thitamadee, S., Tuchihara, K. & Hashimoto, T. Microtubule basis for left-handed helical growth in arabidopsis. *Nature* **417**, 193–196 (2002).
62. Furutani, I. et al. The SPIRAL genes are required for directional control of cell elongation in *Aarabidopsis thaliana*. *Development* **127**, 4443–4453 (2000).
63. Lebreton, G. et al. Molecular to organismal chirality is induced by the conserved myosin 1D. *Science* **362**, 949–952 (2018).
64. Manson, M. D. Dynamic motors for bacterial flagella. *Proc. Natl Acad. Sci. USA* **107**, 11151–11152 (2010).
65. Yuan, J., Fahrner, K. A., Turner, L. & Berg, H. C. Asymmetry in the clockwise and counterclockwise rotation of the bacterial flagellar motor. *Proc. Natl Acad. Sci. USA* **107**, 12846–12849 (2010).
66. Mears, P. J., Koirala, S., Rao, C. V., Golding, I. & Chemla, Y. R. *Escherichia coli* swimming is robust against variations in flagellar number. *eLife* **3**, e01916 (2014).
67. Mathijssen, A. J. T. M. et al. Oscillatory surface rheotaxis of swimming *E. coli* bacteria. *Nat. Commun.* **10**, 3434 (2019).
68. DiLuzio, W. R. et al. *Escherichia coli* swim on the right-hand side. *Nature* **435**, 1271–1274 (2005).
69. Brady, P. & Cummings, M. Differential response to circularly polarized light by the jewel scarab beetle *Chrysina gloriosa*. *Am. Nat.* **175**, 614–620 (2010).
70. Warrant, E. J. Polarisation vision: beetles see circularly polarised light. *Curr. Biol.* **20**, R610–R612 (2010).
71. Cheng, L., Wang, L. & Karlsson, A. M. Image analyses of two crustacean exoskeletons and implications of the exoskeletal microstructure on the mechanical behavior. *J. Mater. Res.* **23**, 2854–2872 (2008).
72. Yang, R., Zaheri, A., Gao, W., Hayashi, C. & Espinosa, H. D. AFM identification of beetle exocuticle: Bouligand structure and nanofiber anisotropic elastic properties. *Adv. Funct. Mater.* **27**, 1603993 (2017).
73. Suksangpanya, N., Yaraghi, N. A., Kisailus, D. & Zavattieri, P. Twisting cracks in bouligand structures. *J. Mech. Behav. Biomed. Mater.* **76**, 38–57 (2017).
74. Chiou, T.-H. et al. Circular polarization vision in a stomatopod crustacean. *Curr. Biol.* **18**, 429–434 (2008).
75. Daly, I. M. et al. Dynamic polarization vision in mantis shrimps. *Nat. Commun.* **7**, 12140 (2016).
76. Natarajan, B. & Gilman, J. W. Bioinspired bouligand cellulose nanocrystal composites: a review of mechanical properties. *Philos. Trans. R. Soc. A Math. Phys. Eng. Sci.* **376**, 20170050 (2018).
77. Zimmermann, E. A. et al. Mechanical adaptability of the Bouligand-type structure in natural dermal armour. *Nat. Commun.* **4**, 2634 (2013).
78. Vignolini, S. et al. Pointillist structural color in pollia fruit. *Proc. Natl Acad. Sci. USA* **109**, 15712–15715 (2012).
79. Visheratina, A., Kumar, P. & Kotov, N. Engineering of inorganic nanostructures with hierarchy of chiral geometries at multiple scales. *AIChE J.* **68**, 17438 (2022).
80. Gianoli, E. The behavioural ecology of climbing plants. *AoB Plants* **7**, plv013 (2015).
81. Smyth, D. R. Helical growth in plant organs: mechanisms and significance. *Development* **143**, 3272–3282 (2016).
82. Wang, J.-S. et al. Hierarchical chirality transfer in the growth of towel gourd tendrils. *Sci. Rep.* **3**, 3102 (2013).
83. Shibazaki, Y., Shimizu, M. & Kuroda, R. Body handedness is directed by genetically determined cytoskeletal dynamics in the early embryo. *Curr. Biol.* **14**, 1462–1467 (2004).
84. Schilthuizen, M. et al. Sexual selection maintains whole-body chiral dimorphism in snails. *J. Evol. Biol.* **20**, 1941–1949 (2007).
85. Suzuki, M., Sasaki, T., Oaki, Y. & Imai, H. Stepwise rotation of nanometric building blocks in the aragonite helix of a pteropod shell. *Cryst. Growth Des.* **17**, 191–196 (2017).
86. Li, L., Weaver, J. C. & Ortiz, C. Hierarchical structural design for fracture resistance in the shell of the pteropod clio pyramidata. *Nat. Commun.* **6**, 6216 (2015).
87. Willinger, M. G., Checa, A. G., Bonarski, J. T., Faryna, M. & Berent, K. Biogenic crystallographically continuous aragonite helices: the microstructure of the planktonic gastropod cuvierina. *Adv. Funct. Mater.* **26**, 553–561 (2016).
88. Jiang, W., Yi, X. & McKee, M. D. Chiral biomineralized structures and their biomimetic synthesis. *Mater. Horiz.* **6**, 1974–1990 (2019).
89. Zhang, T. et al. Structure and mechanical properties of a pteropod shell consisting of interlocked helical aragonite nanofibers. *Angew. Chem. Int. Ed.* **50**, 10361–10365 (2011).
90. Soldati, A. L., Jacob, D. E., Glatzel, P., Swarbrick, J. C. & Geck, J. Element substitution by living organisms: the case of manganese in mollusc shell aragonite. *Sci. Rep.* **6**, 22514 (2016).
91. Eguchi, N. O., Ujiié, H., Kawahata, H. & Taira, A. Seasonal variations in planktonic foraminifera at three sediment traps in the subarctic, transition and subtropical zones of the central north Pacific Ocean. *Mar. Micropaleontol.* **48**, 149–163 (2003).
92. Georgescu, M. D. Evolutionary classification of the upper cretaceous (Turonian–Lower Campanian) planktic foraminifera with incipient meridional ornamentation. *J. Micropalaeontol.* **29**, 149–161 (2010).
93. Addadi, L. & Weiner, S. Crystals, asymmetry and life. *Nature* **411**, 753–755 (2001).
94. Orme, C. A. et al. Formation of chiral morphologies through selective binding of amino acids to calcite surface steps. *Nature* **411**, 775–779 (2001).
95. Kabalah-Amitai, L. et al. Vaterite crystals contain two interspersed crystal structures. *Science* **340**, 454–457 (2013).
96. Jiang, W. et al. Chiral acidic amino acids induce chiral hierarchical structure in calcium carbonate. *Nat. Commun.* **8**, 15066 (2017).
97. Young, J. R. Biomineralization within vesicles: the calcite of coccoliths. *Rev. Mineral. Geochem.* **54**, 189–215 (2003).
98. Branson, O. et al. Nanometer-scale chemistry of a calcite biomineralization template: implications for skeletal composition and nucleation. *Proc. Natl Acad. Sci. USA* **113**, 12934–12939 (2016).
99. Adam, D. Chemistry Nobel 2001. *Nature* https://doi.org/10.1038/news011011-17 (2001).
100. Hananel, U., Ben-Moshe, A., Diamant, H. & Markovich, G. Spontaneous and directed symmetry breaking in the formation of chiral nanocrystals. *Proc. Natl Acad. Sci. USA* **116**, 11159–11164 (2019).
101. Lan, X. & Wang, Q. Self-assembly of chiral plasmonic nanostructures. *Adv. Mater.* **28**, 10499–10507 (2016).
102. Hentschel, M., Schäferling, M., Duan, X., Giessen, H. & Liu, N. Chiral plasmonics. *Sci. Adv.* **3**, e1602735 (2017).

103. Hazen, R. M. & Sholl, D. S. Chiral selection on inorganic crystalline surfaces. *Nat. Mater.* **2**, 367–374 (2003).
104. Hazen, R. M. *Progress in Biological Chirality* (Elsevier, 2004).
105. Sholl, D. S. Adsorption of chiral hydrocarbons on chiral platinum surfaces. *Langmuir* **14**, 862–867 (1998).
106. Ahmadi, A., Attard, G., Feliu, J. & Rodes, A. Surface reactivity at "chiral" platinum surfaces. *Langmuir* **15**, 2420–2424 (1999).
107. Shukla, N. & Gellman, A. J. Chiral metal surfaces for enantioselective processes. *Nat. Mater.* **19**, 939–945 (2020).
This article provides insight into atomic-level inorganic chirality and how such surfaces could be used for enantioselective processes.
108. Im, S. W. et al. Chiral surface and geometry of metal nanocrystals. *Adv. Mater.* **32**, 1905758 (2020).
109. Horvath, J. D. & Gellman, A. J. Enantiospecific desorption of chiral compounds from chiral Cu(643) and achiral Cu(111) surfaces. *J. Am. Chem. Soc.* **124**, 2384–2392 (2002).
110. Fajín, J. L. C., Gomes, J. R. B. & Cordeiro, M. N. D. S. DFT study of the adsorption of D-(L-)cysteine on flat and chiral stepped gold surfaces. *Langmuir* **29**, 8856–8864 (2013).
111. Jadzinsky, P. D., Calero, G., Ackerson, C. J., Bushnell, D. A. & Kornberg, R. D. Structure of a thiol monolayer-protected gold nanoparticle at 1.1 Å resolution. *Science* **318**, 430–433 (2007).
112. Nakashima, T., Kobayashi, Y. & Kawai, T. Optical activity and chiral memory of thiol-capped CdTe nanocrystals. *J. Am. Chem. Soc.* **131**, 10342–10343 (2009).
113. Morales-Vidal, J., López, N. & Ortuño, M. A. Chirality transfer in gold nanoparticles by L-cysteine amino acid: a first-principles study. *J. Phys. Chem. C.* **123**, 13758–13764 (2019).
114. Jiang, W., Pacella, M. S., Vali, H., Gray, J. J. & McKee, M. D. Chiral switching in biomineral suprastructures induced by homochiral L-amino acid. *Sci. Adv.* **4**, eaas9819 (2018).
115. Kulp, E. A. & Switzer, J. A. Electrochemical biomineralization: the deposition of calcite with chiral morphologies. *J. Am. Chem. Soc.* **129**, 15120–15121 (2007).
116. Wang, P. P., Yu, S.-J. J., Govorov, A. O. & Ouyang, M. Cooperative expression of atomic chirality in inorganic nanostructures. *Nat. Commun.* **8**, 14312 (2017).
117. Yeom, J. et al. Chiromagnetic nanoparticles and gels. *Science* **359**, 309–314 (2018).
118. Kim, H. et al. Tyrosyltyrosylcysteine-directed synthesis of chiral cobalt oxide nanoparticles and peptide conformation analysis. *ACS Nano* **15**, 979–988 (2021).
119. Po, H. et al. Chiral helices formation by self-assembled molecules on semiconductor flexible substrates. *ACS Nano* **16**, 2901–2909 (2022).
120. Ben-Moshe, A. et al. Enantioselective control of lattice and shape chirality in inorganic nanostructures using chiral biomolecules. *Nat. Commun.* **5**, 4302 (2014).
121. Ben-Moshe, A. et al. The chain of chirality transfer in tellurium nanocrystals. *Science* **372**, 729–733 (2021).
122. Varanda, L. C. et al. Size- and shape-controlled nanomaterials based on modified polyol and thermal decomposition approaches. A brief review. *An. Acad. Bras. Cienc.* **91**, 04 (2019).
123. Dunne, P. W., Starkey, C. L., Gimeno-Fabra, M. & Lester, E. H. The rapid size- and shape-controlled continuous hydrothermal synthesis of metal sulphide nanomaterials. *Nanoscale* **6**, 2406–2418 (2014).
124. Ahn, H.-Y. Y., Lee, H.-E. E., Jin, K. & Nam, K. T. Extended gold nano-morphology diagram: synthesis of rhombic dodecahedra using CTAB and ascorbic acid. *J. Mater. Chem. C Mater.* **1**, 6861 (2013).
125. Xia, Y., Xia, X. & Peng, H.-C. Shape-controlled synthesis of colloidal metal nanocrystals: thermodynamic versus kinetic products. *J. Am. Chem. Soc.* **137**, 7947–7966 (2015).
126. Grzelczak, M., Pérez-Juste, J., Mulvaney, P. & Liz-Marzán, L. M. Shape control in gold nanoparticle synthesis. *Chem. Soc. Rev.* **37**, 1783 (2008).
127. Hong, J. W., Lee, S.-U. U., Lee, Y. W. & Han, S. W. Hexoctahedral Au nanocrystals with high-index facets and their optical and surface-enhanced Raman scattering properties. *J. Am. Chem. Soc.* **134**, 4565–4568 (2012).
128. Jana, N. R., Gearheart, L. & Murphy, C. J. Seed-mediated growth approach for shape-controlled synthesis of spheroidal and rod-like gold nanoparticles using a surfactant template. *Adv. Mater.* **13**, 1389–1393 (2001).
129. Thambi, V. et al. Synthesis of complex nanoparticle geometries via PH-controlled overgrowth of gold nanorods. *ACS Omega* **4**, 13733–13739 (2019).
130. Personick, M. L. & Mirkin, C. A. Making sense of the mayhem behind shape control in the synthesis of gold nanoparticles. *J. Am. Chem. Soc.* **135**, 18238–18247 (2013).
131. Sau, T. K. & Murphy, C. J. Room temperature, high-yield synthesis of multiple shapes of gold nanoparticles in aqueous solution. *J. Am. Chem. Soc.* **126**, 8648–8649 (2004).
132. Lee, H.-E. E. et al. Concave rhombic dodecahedral Au nanocatalyst with multiple high-index facets for CO_2 reduction. *ACS Nano* **9**, 8384–8393 (2015).
133. Lee, H.-E. et al. Amino-acid- and peptide-directed synthesis of chiral plasmonic gold nanoparticles. *Nature* **556**, 360–365 (2018).
This article reports the use of enantioselective interaction between an inorganic surface and chiral molecules to chemically synthesize 3D chiral gold nanoparticles.
134. Cho, N. H. et al. Uniform chiral gap synthesis for high dissymmetry factor in single plasmonic gold nanoparticle. *ACS Nano* **14**, 3595–3602 (2020).
135. Lee, H.-E. et al. Cysteine-encoded chirality evolution in plasmonic rhombic dodecahedral gold nanoparticles. *Nat. Commun.* **11**, 263 (2020).
136. Lee, Y. Y. et al. Chiral 432 helicoid ii nanoparticle synthesized with glutathione and poly(T)20 nucleotide. *ChemNanoMat* **6**, 362–367 (2020).
137. Kim, H. et al. γ-Glutamylcysteine- and cysteinylglycine-directed growth of chiral gold nanoparticles and their crystallographic analysis. *Angew. Chem. Int. Ed.* **59**, 12976–12983 (2020).
138. Cho, N. H. et al. Adenine oligomer directed synthesis of chiral gold nanoparticles. *Nat. Commun.* **13**, 3831 (2022).
139. Cho, N. H. et al. Cysteine induced chiral morphology in palladium nanoparticle. *Part. Part. Syst. Charact.* **36**, 1900062 (2019).
140. Wennerström, H. Micelles. Physical chemistry of surfactant association. *Phys. Rep.* **52**, 1–86 (1979).
141. van Meer, G., Voelker, D. R. & Feigenson, G. W. Membrane lipids: where they are and how they behave. *Nat. Rev. Mol. Cell Biol.* **9**, 112–124 (2008).
142. Holmberg, K. Surfactant-templated nanomaterials synthesis. *J. Colloid Interface Sci.* **274**, 355–364 (2004).
143. Seddon, A. M., Patel, H. M., Burkett, S. L. & Mann, S. Chiral templating of silica-lipid lamellar mesophase with helical tubular architecture. *Angew. Chem. Int. Ed.* **41**, 2988–2991 (2002).
144. Bordes, R. & Holmberg, K. Amino acid-based surfactants — do they deserve more attention? *Adv. Colloid Interface Sci.* **222**, 79–91 (2015).
145. Qiu, H. & Che, S. Formation mechanism of achiral amphiphile-templated helical mesoporous silicas. *J. Phys. Chem. B* **112**, 10466–10474 (2008).
146. Ito, T. H. et al. Generation of a chiral giant micelle. *Langmuir* **32**, 8461–8466 (2016).
147. Delclos, T. et al. Individualized silica nanohelices and nanotubes: tuning inorganic nanostructures using lipidic self-assemblies. *Nano Lett.* **8**, 1929–1935 (2008).
148. Yang, S. et al. On the origin of helical mesostructures. *J. Am. Chem. Soc.* **128**, 10460–10466 (2006).
149. Peng, L. et al. Spiral self-assembly of lamellar micelles into multi-shelled hollow nanospheres with unique chiral architecture. *Sci. Adv.* **7**, eabi7403 (2021).
150. Jin, H. et al. Control of morphology and helicity of chiral mesoporous silica. *Adv. Mater.* **18**, 593–596 (2006).
151. Che, S. et al. Synthesis and characterization of chiral mesoporous silica. *Nature* **429**, 281–284 (2004).
This article demonstrates the mineralization of chiral micelles into silica nanostructures with defined chiral morphologies.
152. Wang, B. et al. Chiral mesostructured silica nanofibers of MCM-41. *Angew. Chem. Int. Ed.* **45**, 2088–2090 (2006).
153. Han, Y., Zhao, L. & Ying, J. Y. Entropy-driven helical mesostructure formation with achiral cationic surfactant templates. *Adv. Mater.* **19**, 2454–2459 (2007).
154. Zhong, S.-L., Zhang, L.-F. & Xu, A.-W. Entropically driven formation of ultralong helical mesostructured organosilica nanofibers. *Small* **10**, 888–894 (2014).
155. Liu, S. et al. Synthesis of chiral TiO_2 nanofibre with electron transition-based optical activity. *Nat. Commun.* **3**, 1215 (2012).
156. Duan, Y. et al. Optically active chiral CuO "nanoflowers." *J. Am. Chem. Soc.* **136**, 7193–7196 (2014).
157. Qian, Y., Duan, Y. & Che, S. Chiral nanostructured CuO films with multiple optical activities. *Adv. Opt. Mater.* **5**, 1601013 (2017).
158. Jana, N. R., Gearheart, L. & Murphy, C. J. Wet chemical synthesis of high aspect ratio cylindrical gold nanorods. *J. Phys. Chem. B* **105**, 4065–4067 (2001).
159. González-Rubio, G. et al. Disconnecting symmetry breaking from seeded growth for the reproducible synthesis of high quality gold nanorods. *ACS Nano* **13**, 4424–4435 (2019).
160. González-Rubio, G. et al. Micelle-directed chiral seeded growth on anisotropic gold nanocrystals. *Science* **368**, 1472–1477 (2020).
This article reports the use of mixed chiral micelles as a template for the synthesis of chiral gold nanorods that exhibit plasmon modes with high dissymmetry factors.
161. Heyvaert, W. et al. Quantification of the helical morphology of chiral gold nanorods. *ACS Mater. Lett.* **4**, 642–649 (2022).
162. Guerrero-Martínez, A., Pérez-Juste, J., Carbó-Argibay, E., Tardajos, G. & Liz-Marzán, L. M. Gemini-surfactant-directed self-assembly of monodisperse gold nanorods into standing superlattices. *Angew. Chem. Int. Ed.* **48**, 9484–9488 (2009).
163. Fernández, C. et al. Nucleation of amyloid oligomers by RepA-WH1-prionoid-functionalized gold nanorods. *Angew. Chem. Int. Ed.* **55**, 11237–11241 (2016).
164. Noorduin, W. L. et al. Complete chiral symmetry breaking of an amino acid derivative directed by circularly polarized light. *Nat. Chem.* **1**, 729–732 (2009).
165. Shibata, T. et al. Amplification of a slight enantiomeric imbalance in molecules based on asymmetric autocatalysis: the first correlation between high enantiomeric enrichment in a chiral molecule and circularly polarized light. *J. Am. Chem. Soc.* **120**, 12157–12158 (1998).
166. Wu, W. & Pauly, M. Chiral plasmonic nanostructures: recent advances in their synthesis and applications. *Mater. Adv.* **3**, 186–215 (2022).
167. Srivastava, S. et al. Light-controlled self-assembly of semiconductor nanoparticles into twisted ribbons. *Science* **327**, 1355–1359 (2010).
168. Lilly, G. D., Agarwal, A., Srivastava, S. & Kotov, N. A. Helical assemblies of gold nanoparticles. *Small* **7**, 2004–2009 (2011).
169. Yeom, J. et al. Chiral templating of self-assembling nanostructures by circularly polarized light. *Nat. Mater.* **14**, 66–72 (2015).
170. Wang, H. et al. Selectively regulating the chiral morphology of amino acid-assisted chiral gold nanoparticles with circularly polarized light. *ACS Appl. Mater. Interfaces* **14**, 3559–3567 (2022).
171. Harutyunyan, H. et al. Anomalous ultrafast dynamics of hot plasmonic electrons in nanostructures with hot spots. *Nat. Nanotechnol.* **10**, 770–774 (2015).
172. Straney, P. J. et al. Ligand-mediated deposition of noble metals at nanoparticle plasmonic hotspots. *Langmuir* **34**, 1084–1091 (2018).

173. Xu, L. et al. Enantiomer-dependent immunological response to chiral nanoparticles. *Nature* **601**, 366–373 (2022).
This article provides an example for applications of chiral nanotechnology in immunology, and shows how chiral particles could function as vaccine adjuvants.
174. Tian, Y. & Tatsuma, T. Mechanisms and applications of plasmon-induced charge separation at TiO_2 films loaded with gold nanoparticles. *J. Am. Chem. Soc.* **127**, 7632–7637 (2005).
175. Saito, K. & Tatsuma, T. Chiral plasmonic nanostructures fabricated by circularly polarized light. *Nano Lett.* **18**, 3209–3212 (2018).
176. Morisawa, K., Ishida, T. & Tatsuma, T. Photoinduced chirality switching of metal–inorganic plasmonic nanostructures. *ACS Nano* **14**, 3603–3609 (2020).
This article reports a chiral gold nanocuboid, with CPL as the only source of chirality, with reversible deposition of lead oxide, which allows chirality to be modulated only by light.
177. Besteiro, L. V. et al. Local growth mediated by plasmonic hot carriers: chirality from achiral nanocrystals using circularly polarized light. *Nano Lett.* **21**, 10315–10324 (2021).
This article reports computational models that describe the mechanisms for growing a chiral gold nanoparticle without the use of chiral ligands.
178. Kim, J.-Y. et al. Assembly of gold nanoparticles into chiral superstructures driven by circularly polarized light. *J. Am. Chem. Soc.* **141**, 11739–11744 (2019).
179. Ayuso, D. et al. Synthetic chiral light for efficient control of chiral light–matter interaction. *Nat. Photonics* **13**, 866–871 (2019).
180. Spreyer, F. et al. Second harmonic optical circular dichroism of plasmonic chiral helicoid-III nanoparticles. *ACS Photonics* **9**, 784–792 (2022).
181. Yan, J. et al. Self-assembly of chiral nanoparticles into semiconductor helices with tunable near-infrared optical activity. *Chem. Mater.* **32**, 476–488 (2020).
182. Ohnoutek, L. et al. Third-harmonic Mie scattering from semiconductor nanohelices. *Nat. Photonics* **16**, 126–133 (2022).
183. Zheng, G. et al. Discrete metal nanoparticles with plasmonic chirality. *Chem. Soc. Rev.* **50**, 3738–3754 (2021).
184. Zhang, L., Xu, C., Liu, C. & Li, B. Visual chiral recognition of tryptophan enantiomers using unmodified gold nanoparticles as colorimetric probes. *Anal. Chim. Acta* **809**, 123–127 (2014).
185. Zhang, M. & Ye, B.-C. Colorimetric chiral recognition of enantiomers using the nucleotide-capped silver nanoparticles. *Anal. Chem.* **83**, 1504–1509 (2011).
186. Song, G., Xu, C. & Li, B. Visual chiral recognition of mandelic acid enantiomers with L-tartaric acid-capped gold nanoparticles as colorimetric probes. *Sens. Actuators B Chem.* **215**, 504–509 (2015).
187. Song, L., Wang, S., Kotov, N. A. & Xia, Y. Nonexclusive fluorescent sensing for L/D enantiomers enabled by dynamic nanoparticle-nanorod assemblies. *Anal. Chem.* **84**, 7330–7335 (2012).
188. Tang, L. et al. Chirality-based Au@Ag nanorod dimers sensor for ultrasensitive PSA detection. *ACS Appl. Mater. Interfaces* **7**, 12708–12712 (2015).
189. Matuschek, M. et al. Chiral plasmonic hydrogen sensors. *Small* **14**, 1702990 (2018).
190. Su, H., Zheng, Q. & Li, H. Colorimetric detection and separation of chiral tyrosine based on *N*-acetyl-L-cysteine modified gold nanoparticles. *J. Mater. Chem.* **22**, 6546 (2012).
191. Miles, A. J., Janes, R. W. & Wallace, B. A. Tools and methods for circular dichroism spectroscopy of proteins: a tutorial review. *Chem. Soc. Rev.* **50**, 8400–8413 (2021).
192. di Gregorio, M. C., Ben Moshe, A., Tirosh, E., Galantini, L. & Markovich, G. Chiroptical study of plasmon–molecule interaction: the case of interaction of glutathione with silver nanocubes. *J. Phys. Chem. C.* **119**, 17111–17116 (2015).
193. Jeong, H.-H. et al. Dispersion and shape engineered plasmonic nanosensors. *Nat. Commun.* **7**, 11331 (2016).
194. Cai, J. et al. Chiral shell core-satellite nanostructures for ultrasensitive detection of mycotoxin. *Small* **14**, 1703931 (2018).
195. Sachs, J., Günther, J.-P., Mark, A. G. & Fischer, P. Chiroptical spectroscopy of a freely diffusing single nanoparticle. *Nat. Commun.* **11**, 4513 (2020).
196. Ma, W. et al. Detection with chiral nanorod assemblies. *Nat. Commun.* **4**, 2689 (2013).
197. Kakkanattu, A., Eerqing, N., Ghamari, S. & Vollmer, F. Review of optical sensing and manipulation of chiral molecules and nanostructures with the focus on plasmonic enhancements [Invited]. *Opt. Express* **29**, 12543 (2021).
198. Marinakos, S. M., Chen, S. & Chilkoti, A. Plasmonic detection of a model analyte in serum by a gold nanorod sensor. *Anal. Chem.* **79**, 5278–5283 (2007).
199. Li, S. et al. Single- and multi-component chiral supraparticles as modular enantioselective catalysts. *Nat. Commun.* **10**, 4826 (2019).
200. Wu, F. et al. Synthesis of chiral Au nanocrystals with precise homochiral facets for enantioselective surface chemistry. *Nano Lett.* **22**, 2915–2922 (2022).
201. Wattanakit, C. et al. Enantioselective recognition at mesoporous chiral metal surfaces. *Nat. Commun.* **5**, 3325 (2014).
202. Yutthalekha, T. et al. Asymmetric synthesis using chiral-encoded metal. *Nat. Commun.* **7**, 12678 (2016).
203. Zhang, H. et al. Engineering of chiral nanomaterials for biomimetic catalysis. *Chem. Sci.* **11**, 12937–12954 (2020).
204. Tan, L., Yu, S., Jin, Y., Li, J. & Wang, P. Inorganic chiral hybrid nanostructures for tailored chiroptics and chirality-dependent photocatalysis. *Angew. Chemie Int. Ed.* **61**, e202112400 (2022).
205. Wei, X. et al. Enantioselective photoinduced cyclodimerization of a prochiral anthracene derivative adsorbed on helical metal nanostructures. *Nat. Chem.* **12**, 551–559 (2020).
206. Sun, M. et al. Site-selective photoinduced cleavage and profiling of DNA by chiral semiconductor nanoparticles. *Nat. Chem.* **10**, 821–830 (2018).
207. Li, F. et al. Chiral carbon dots mimicking topoisomerase I to mediate the topological rearrangement of supercoiled DNA enantioselectively. *Angew. Chem. Int. Ed.* **59**, 11087–11092 (2020).
208. Smith, A. M., Mancini, M. C. & Nie, S. Second window for in vivo imaging. *Nat. Nanotechnol.* **4**, 710–711 (2009).
209. Li, Y. et al. A visible- and NIR-light responsive photothermal therapy agent by chirality-dependent MoO_{3-x} nanoparticles. *Adv. Funct. Mater.* **30**, 1906311 (2020).
210. Zhang, M., Zhang, H., Feng, J., Zhou, Y. & Wang, B. Synergistic chemotherapy, physiotherapy and photothermal therapy against bacterial and biofilms infections through construction of chiral glutamic acid functionalized gold nanobipyramids. *Chem. Eng. J.* **393**, 124778 (2020).
This article describes chiral nanomaterials that can aid in wound healing following *S. epidermidis* infections in mice.
211. Fan, Y., Ou-yang, S., Zhou, D., Wei, J. & Liao, L. Biological applications of chiral inorganic nanomaterials. *Chirality* **34**, 760–781 (2022).
212. Chen, D. S. & Mellman, I. Oncology meets immunology: the cancer–immunity cycle. *Immun. Cycle. Immun.* **39**, 1–10 (2013).
213. Kakkar, T. et al. Superchiral near fields detect virus structure. *Light. Sci. Appl.* **9**, 195 (2020).
214. Goerlitzer, E. S. A. et al. Chiral surface lattice resonances. *Adv. Mater.* **32**, 2001330 (2020).
215. Choo, P. et al. Investigating reaction intermediates during the seedless growth of gold nanostars using electron tomography. *ACS Nano* **16**, 4408–4414 (2022).
216. Winckelmans, N. et al. Multimode electron tomography as a tool to characterize the internal structure and morphology of gold nanoparticles. *J. Phys. Chem. C.* **122**, 13522–13528 (2018).
217. Haberfehlner, G. et al. 3D imaging of gap plasmons in vertically coupled nanoparticles by EELS tomography. *Nano Lett.* **17**, 6773–6777 (2017).
218. Schwartz, J. et al. Real-time 3D analysis during electron tomography using tomviz. *Nat. Commun.* **13**, 4458 (2022).
219. Bals, S., Goris, B., De Backer, A., Van Aert, S. & Van Tendeloo, G. Atomic resolution electron tomography. *MRS Bull.* **41**, 525–530 (2016).
220. Zhou, J., Yang, Y., Ercius, P. & Miao, J. Atomic electron tomography in three and four dimensions. *MRS Bull.* **45**, 290–297 (2020).
221. Midgley, P. A. & Weyland, M. 3D electron microscopy in the physical sciences: the development of Z-contrast and EFTEM tomography. *Ultramicroscopy* **96**, 413–431 (2003).
222. Milagres de Oliveira, T. et al. 3D characterization and plasmon mapping of gold nanorods welded by femtosecond laser irradiation. *ACS Nano* **14**, 12558–12570 (2020).
223. Goris, B. et al. Measuring lattice strain in three dimensions through electron microscopy. *Nano Lett.* **15**, 6996–7001 (2015).
224. Inada, H. et al. Atomic resolution secondary electron imaging in aberration corrected STEM. *Microsc. Anal.* **25**, S5–S8 (2011).
225. Rogolino, A. et al. Metal–polymer heterojunction in colloidal-phase plasmonic catalysis. *J. Phys. Chem. Lett.* **13**, 2264–2272 (2022).
226. Karst, J., Strohfeldt, N., Schäferling, M., Giessen, H. & Hentschel, M. Single plasmonic oligomer chiral spectroscopy. *Adv. Opt. Mater.* **6**, 1800087 (2018).
227. Karst, J. et al. Chiral scatterometry on chemically synthesized single plasmonic nanoparticles. *ACS Nano* **13**, 8659–8668 (2019).
228. Choo, P., Liu, T. & Odom, T. W. Nanoparticle shape determines dynamics of targeting nanoconstructs on cell membranes. *J. Am. Chem. Soc.* **143**, 4550–4555 (2021).
229. Cha, M. et al. Unifying structural descriptors for biological and bioinspired nanoscale complexes. *Nat. Comput. Sci.* **2**, 243–252 (2022).
230. Wang, W. Imaging the chemical activity of single nanoparticles with optical microscopy. *Chem. Soc. Rev.* **47**, 2485–2508 (2018).
231. Vecchio, D. A., Mahler, S. H., Hammig, M. D. & Kotov, N. A. Structural analysis of nanoscale network materials using graph theory. *ACS Nano* **15**, 12847–12859 (2021).
232. Manukyan, L., Montandon, S. A., Fofonjka, A., Smirnov, S. & Milinkovitch, M. C. A living mesoscopic cellular automaton made of skin scales. *Nature* **544**, 173–179 (2017).
This article reports a cellular automation method for analysing skin microstructures of ocellated lizards, shedding light on evolutionary mechanisms.
233. Alkhazraji, E., Ghalib, A., Manzoor, K. & Alsunaidi, M. A. Plasmonic nanostructured cellular automata. *EPJ Web Conf.* **139**, 00001 (2017).
234. Cha, S.-H. et al. Shape-dependent biomimetic inhibition of enzyme by nanoparticles and their antibacterial activity. *ACS Nano* **9**, 9097–9105 (2015).
235. Weisberg, S. B. et al. Water quality criteria for an acidifying ocean: challenges and opportunities for improvement. *Ocean Coast Manag.* **126**, 31–41 (2016).
236. Shafik, S., Watkins, D. K. & Shin, I. C. in *Proc. Ocean Drilling Program, Scientific Results* Vol. 159 (eds Mascle, J., Lohmann, G. P. & Moullade, M.) 413–431 (Ocean Drilling Program, 1998).

Acknowledgements

The authors acknowledge support by the Creative Materials Discovery Program through the National Research Foundation of Korea (NRF) funded by Ministry of Science and ICT (NRF-2017M3D1A1039377), the LG Display under LGD-SNU Incubation Program, the Spanish Ministry of Science, Innovation and Universities (MICIU) (Grant No. RTI2018-095844-B-I00), the Madrid Regional Government (Grant Nos. P2018/NMT-4389 and REACT ANTICIPA-UCM), the Office of Naval Research via Vannevar Bush DoD Fellowship to N.A.K. titled 'Engineered

Chiral Ceramics' (ONR N000141812876), MURI N00014-20-1-2479 and COVID-19 Newton Award 'Pathways to Complexity with "Imperfect" NPs' (HQ00342010033). Part of this work was also supported by AFOSR FA9550-20-1-0265, Graph Theory Description of Network Material.

Author contributions

N.H.C., J.M. and A.G.-M. wrote the manuscript and contributed equally. S.B. contributed a perspective on tomographic analysis of chiral nanomaterials. N.A.K., L.M.L.-M. and K.T.N. wrote the manuscript and guided all aspects of the work.

Competing interests

The authors declare no competing interests.

Additional information

Correspondence should be addressed to Nicholas A. Kotov, Luis M. Liz-Marzán or Ki Tae Nam.

Peer review information *Nature Reviews Bioengineering* thanks Zhiqun Lin and the other, anonymous, reviewer(s) for their contribution to the peer review of this work.